Macromolecules
ARTICLE

Macromolecules **2010**, *43*, 4921–4936 **4921**
DOI: 10.1021/ma902432m

Hyperbranched Conjugated Polysiloles: Synthesis, Structure, Aggregation-Enhanced Emission, Multicolor Fluorescent Photopatterning, and Superamplified Detection of Explosives

Jianzhao Liu,[†,§] Yongchun Zhong,[‡] Jacky W. Y. Lam,[†,§] Ping Lu,[†,§] Yuning Hong,[†,§] Yong Yu,[†,§] Yanan Yue,[⊥] Mahtab Faisal,[†,§] Herman H. Y. Sung,[†] Ian D. Williams,[†] Kam Sing Wong,[‡] and Ben Zhong Tang*[,†,§,∥]

[†]*Department of Chemistry, Institute of Molecular Functional Materials,* [‡]*Department of Physics, The Hong Kong University of Science & Technology (HKUST), Clear Water Bay, Kowloon, Hong Kong, China,* [§]*HKUST Fok Ying Tung Research Institute, Nansha, Guangzhou, China,* [⊥]*Department of Chemistry, The Chinese University of Hong Kong, Shatin, New Territories, Hong Kong, China, and* [∥]*Department of Polymer Science and Engineering, Zhejiang University, Hangzhou 310027, China*

Received November 2, 2009; Revised Manuscript Received April 20, 2010

ABSTRACT: Hyperbranched poly(2,5-silole)s [*hb*-**P1**(*m*), $m = 1, 6$] are synthesized for the first time in this work. 1,1-Dialkyl-2,5-bis(4-ethynylphenyl)-3,4-diphenylsiloles [**1**(*m*)] were polymerized by $TaBr_5$, affording *hb*-**P1**(*m*) with high molecular weights (M_w up to 2.5×10^5) in high yields (up to 98%). The structures of *hb*-**P1**(*m*) were characterized by spectroscopic methods and the degree of branching of *hb*-**P1**(6) was determined to be 0.55. The hyperbranched polymers are soluble and stable, with no changes in solubility observed after they have been stored under ambient conditions for more than two years. Absorption and emission spectra of *hb*-**P1**(*m*) are red-shifted from those of **1**(*m*), indicating that the polymers are more conjugated than the monomers. Both **1**(*m*) and *hb*-**P1**(*m*) are nonemissive or weekly fluorescent when dissolved in their good solvents but become highly emissive when aggregated in their poor solvents or fabricated into thin solid films, showing unusual phenomena of aggregation-induced (AIE) and -enhanced emissions (AEE). Restriction of intramolecular rotations in the aggregate state is rationalized to be the main cause for the AIE and AEE effects. Photoluminescence (PL) of **1**(*m*) and *hb*-**P1**(*m*) is tunable by varying their concentrations and morphologies. The polymers are readily cured when heated to high temperatures or upon photoirradiation, furnishing cross-linked networks with novel excitation wavelength-dependent emissions in the red spectral region. Photolithography of *hb*-**P1**(*m*) generates fluorescent photopatterns, with the exposed and unexposed areas emitting lights with different colors. The polymers function as sensitive fluorescent chemosensors for the detection of explosives, with a superamplification effect observed in the emission quenching of the polymer nanoaggregates by picric acid.

Introduction

Development of efficient luminescent materials is of academic interest and practical value. A thorny obstacle against the development is the aggregation-caused quenching (ACQ) effect: in the condensed phase, the luminogenic molecules are located in the immediate vicinity, which promotes the formation of such detrimental species as excimers and exciplexes, leading to undesired radiationless transitions.[1] Various chemical, physical, and engineering approaches and processes have been taken to hamper the aggregate formation and to mitigate the ACQ effect, but the attempts have met with only limited success. In most cases, aggregation is impeded only partially or temporarily. If a system can be developed in which light emission is enhanced, rather than quenched, by aggregation, it would be very rewarding. This will make life much easier because no hard work is needed to artificially interrupt the very natural process of luminogen aggregation.

In 2001, our research groups discovered such a system in which a series of silole molecules were found nonemissive in the solution state but highly luminescent in the aggregate state.[2,3] We coined "aggregation-induced emission" (AIE) for this novel phenomenon because the nonemissive luminogens were induced to emit efficiently by aggregate formation. In the AIE system, the luminogen aggregation plays a constructive, instead of destructive, role in the light-emitting process. Through experimental[3,4] and theoretical studies,[5] the restriction of intramolecular rotations (RIR) in the aggregate state has been identified as a main cause for the AIE effect. In solutions, active rotations of the peripheral phenyl rings (rotors) against the central silacyclopentadiene core (stator) effectively annihilate the excited states, thus making the silole molecules weakly luminescent or nonemissive. The activation of the RIR process by cooling, thickening, pressurization, crystallization, etc. blocks the nonradiative relaxation channels and populates the radiative excitons, thereby turning "on" the emission of the luminogens.[3]

Attracted by the novel AIE effect, our and other research groups have worked on the exploration of technological applications of the AIE luminogens as chemosensors, bioprobes, immunoassay markers, stimuli-responsive materials, solid-state emitters, and so on.[6] Organic light-emitting diodes (OLEDs) have been fabricated from the AIE luminogens, some of which showed outstanding electroluminescence performances. For example, an OLED constructed from 1,1,2,3,4,5-hexaphenylsilole

*Corresponding author. Telephone: +852-2358-7375. Fax: +852-2358-1594. E-mail: tangbenz@ust.hk.

© 2010 American Chemical Society
Published on Web 05/12/2010

(HPS; Chart 1) emits brilliantly (luminance up to ~60000 cd/m^2),[4] while that from 1-methyl-1,2,3,4,5-pentaphenylsilole (MPPS) shows an extremely high external quantum efficiency (8%),[7] reaching the theoretical limit for an OLED based on a singlet emitter.

The silole luminogens are low molecular weight (MW) compounds and have to be fabricated into thin solid films by expensive techniques such as vacuum vapor deposition, which are not well suited to the manufacture of large area devices. One way to overcome this processing disadvantage is to prepare high MW polymers, which can be readily processed from their solutions into thin solid films over large areas by a simple process of spin-coating. Several research groups have worked on the synthesis of silole-containing polymers and the resultant polysiloles have been found to exhibit unique properties, such as narrow energy band gap, efficient photoluminescence (PL), rapid electrochemical switching, and high electron mobility.[8] So far, most of the polysiloles have been prepared by coupling polymerizations. Such reactions, however, require stringent stoichiometric balances of comonomer feeds. This technical difficulty has made the synthesis of high MW polysiloles a challenging task. Almost all the polysiloles are linear macromolecules. The synthesis of their hyperbranched counterparts with three-dimensional architectures remains to be virtually unexplored.

Our research groups have been working on the synthesis of conjugated polymers in the past few decades.[9] Utilizing monoynes and triynes as monomeric building blocks, we have prepared a wide variety of linear polyacetylenes and hyperbranched polytriazoles and polydiynes by metathesis,[10] click,[11] and coupling[12] polymerizations. We have also synthesized a large number of hyperbranched polyarylenes by diyne polycyclotrimerizations of A_2-type monomers.[13,14] The remarkable feature of the polycyclotrimerization is that it does not require stoichiometric balance of the diyne monomers and can thus produce polymers with very high MWs. Because aromatic rings are the basic constituent units, the polymers are thermally very stable [with degradation temperature (T_d) up to ~600 °C] and can efficiently emit intense blue light upon photoexcitation and function as excellent optical limiters when irradiated with harsh laser pulses.[9]

Silole possesses a highly branched molecular structure and exhibits the novel AIE effect and excellent solubility arising from the large volume of its sp^3-hybridized silicon bridge in the silacyclopentadiene ring. Its highest occupied (HOMO) and lowest unoccupied molecular orbitals (LUMO) are mainly localized on the silacyclopentadiene ring and two substituent groups at the 2,5-positions,[6g] through which electronic conjugation can be extended. These unique structural attributes make silole an ideal building block for the construction of hyperbranched polymers. In this work, we synthesized 2,5-diethynylsiloles **1**(*m*) and successfully transformed them into hyperbranched poly(2,5-silole)s *hb*-**P1**(*m*) (Scheme 2) with three-dimensional topological structures and extended electronic conjugations (Chart 2). The polymers have high MWs, are completely soluble, very stable and readily processable (film-forming), and show a novel

Chart 1. HPS and MPPS: Two Archetypal AIE Luminogens

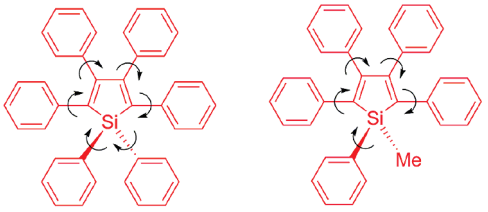

Scheme 2. Thermo- and Photo-Induced Cross-Linking of *hb*-P1(*m*)

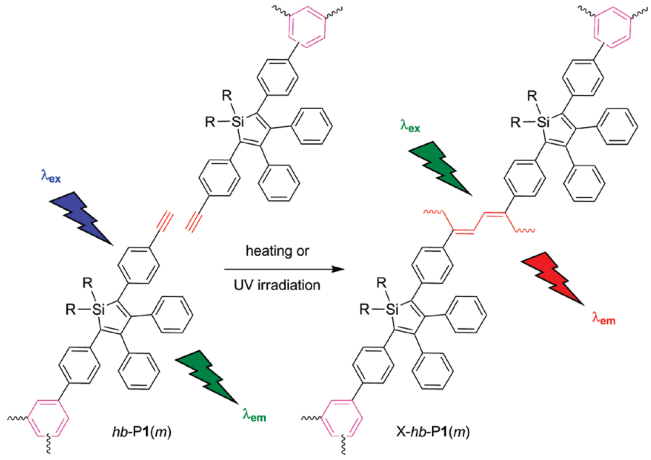

Scheme 1. Syntheses of 2,5-Diethynylsiloles 1(*m*) and Transformations of the Monomers into Hyperbranched Polysiloles P1(*m*) via Diyne Polycyclotrimerization

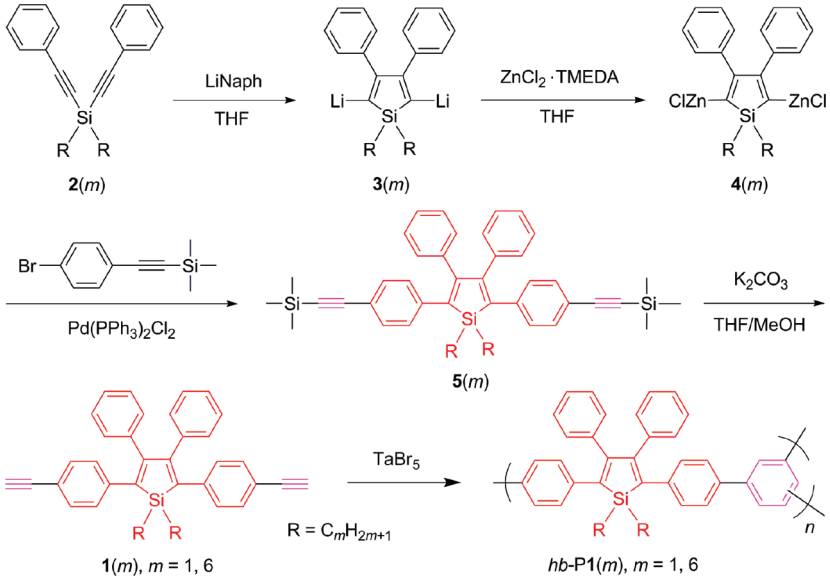

Chart 2. Structures of Dendritic, Linear, and Terminal Units in *hb*-P1(*m*)

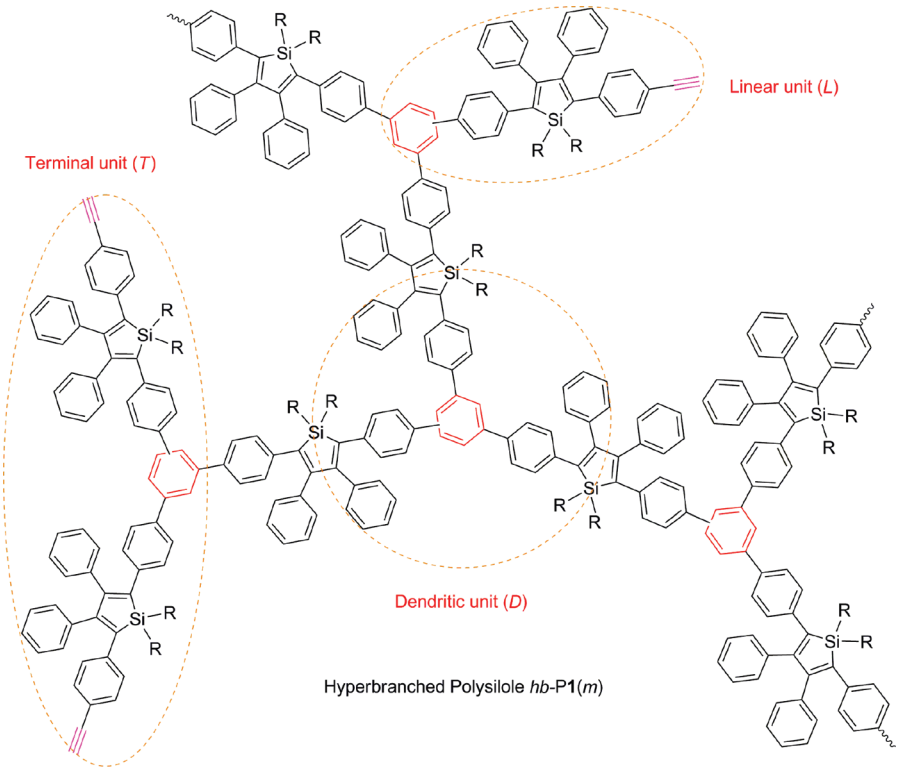

phenomenon of aggregation-enhanced emission (AEE). Utilizing the AEE effect, we explored the high-tech applications of *hb*-P**1**(*m*) as multicolor light-emitting photoresists and fluorescent chemosensor for explosive detection.

Results and Discussion

Monomer Preparation. Since the synthesis of the first silole compound, HPS, was reported in the late 1950s,[15] studies on the preparations, structures and properties of silole molecules have been a topic of intense interest among scientists, especially synthetic chemists.[16,17] The synthetic schemes developed by Tamao and Yamaguchi have become the general routes to silole derivatives.[16−18] In this work, we prepared monomers **1**(*m*) (*m* = 1, 6) in satisfactory yields, using the published experimental procedures with some modifications (Scheme 1).[18b] In this multistep reaction scheme, diethynylsilanes **2**(*m*) undergo intramolecular reductive cyclization in an *endo*−*endo* mode by the treatment with lithium 1-naphthalenide (LiNaph) to form 2,5-dilithiosiloles **3**(*m*), which is transformed to 2,5-dizinc siloles **4**(*m*) by the transmetalation with $ZnCl_2$·TMEDA (TMEDA = *N*,*N*,*N*′,*N*′-tetramethylethylenediamine). The subsequent reaction of **4**(*m*) with (4-bromophenylethynyl)trimethylsilane in the presence of a palladium catalyst yields **5**(*m*). The base-catalyzed desilylation of **5**(*m*) in methanolic K_2CO_3 solution furnishes the desired products **1**(*m*).

The silole monomers were isolated, purified and characterized by standard spectroscopic techniques, from which satisfactory analysis data corresponding to their expected chemical structures were obtained (see Experimental Section for detailed spectroscopic data). Whereas the monomer carrying long *n*-hexyl groups at the 1,1-positions [**1**(6)] is a viscous liquid, its counterpart with short methyl substituents [**1**(1)] is a solid. High-quality single crystals of **1**(1) were successfully grown from a mixture of THF/ethanol. The molecular structure of **1**(1) was determined by analyzing the crystals with the X-ray diffractogram (Supporting Information, Table 1).

Table 1. Polymerizations of 2,5-Diethynylsiloles 1(*m*)[a]

no.	monomer	[cat.] (mM)	time (h)	yield (%)	$M_{w,r}$[b] ($M_{w,a}$)[c]	M_w/M_n[b]
1	**1**(1)	2.5	1	87.3	17400	3.3
2	**1**(1)	5	0.5	75.6	17600 (238000)	3.2
3	**1**(6)	2.5	2	97.9	27600 (249000)	4.1
4	**1**(6)	5	0.5	81.7	52600	6.4
5	**1**(6)	7.5	0.25	84.5	22200	1.9

[a] Carried out in toluene at room temperature under nitrogen using $TaBr_5$ as catalyst; $[M]_0$ = 0.05 M. [b] Relative weight-average molecular weight ($M_{w,r}$) and polydispersity index (M_w/M_n) determined by gel permeation chromatography (GPC) in THF on the basis of linear polystyrenes calibration. [c] Absolute weight-average molecular weights ($M_{w,a}$) determined by static laser light-scattering technique.

Polymer Synthesis. In our previous work, we have systematically investigated the effects of reaction conditions on the polycyclotrimerizations of diyne monomers catalyzed by tantalum halides and found that high MW polymers could be obtained in high yields when the polymerization reactions were carried out in nonpolar solvents, at high temperatures and catalyst and monomer concentrations for prolonged periods of time.[13] The study offers us constructive guidance to polymerize **1**(*m*) under optimal reaction conditions. We first carried out the polymerization of **1**(1) catalyzed by $TaBr_5$ in toluene at a catalyst concentration of 2.5 mM. After stirring at room temperature for 1 h, a soluble polymer product with a relative weight-average MW of 17400 was isolated in a yield of ~87% (Table 1, no. 1). Doubling the catalyst concentration helps shorten the reaction time at no cost of polymerization results (Supporting Information, Figure S1). Similar polymerization behaviors were observed for **1**(6). It should be pointed out that MW of a hyperbranched polymer measured by the GPC system calibrated by linear polystyrene standards is often underestimated, due to the rigid globular architecture of hyperbranched

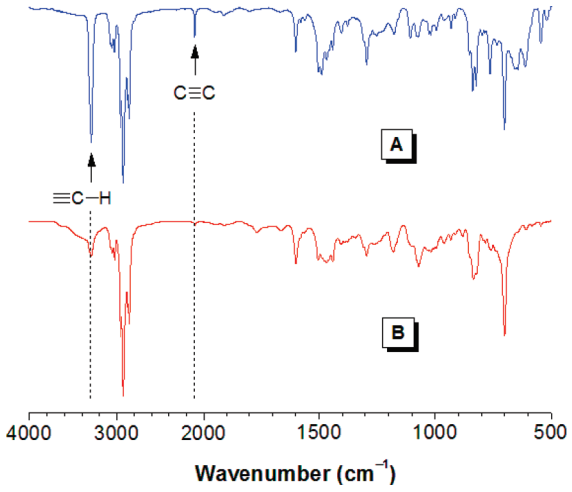

Figure 1. IR spectra of (A) monomer **1**(6) and (B) its polymer *hb*-P**1**(6) (sample taken from Table 1, no. 3).

polymer.[19] Indeed, when MWs of *hb*-P**1**(*m*) were measured by a static laser light-scattering method, their absolute M_w values are 9−13 times higher than the polystyrene-calibrated relative ones (Table 1, nos. 2 and 3). Evidently, the polycyclotrimerizations of **1**(*m*) can produce *hb*-P**1**(*m*) with high MWs in high yields.

All the polymer products are highly soluble in common organic solvents, such as THF, toluene, dichloromethane (DCM), and chloroform, thanks to the large free volumes in the polymers contributed from the twisted propeller-shaped silole repeat units. The polymers remain completely soluble and show excellent optical spectral stability after they have been stored in air in vials under normal room lighting for more than 2 years. This is very different from our previously prepared hyperbranched polyarylenes, which are highly soluble when they have been freshly prepared but become poorly soluble after storage, possibly due to the postpolymerizations of the peripheral triple-bond functional groups coupled with the strong intermolecular $\pi-\pi$ stacking interactions between the aromatic repeat units. The present study thus provides a designing guidance to the synthesis of new hyperbranched polymers with macroscopic processability.

Structural Characterizations. The polymer products were fully characterized spectroscopically (see Experimental Section for detailed analysis data). The IR spectrum of *hb*-P**1**(6) is given in Figure 1 as an example. The spectrum of its monomer **1**(6) is also shown in the same figure for the sake of comparison. The ≡C−H stretching vibration of **1**(6) is observed at 3294 cm^{-1}, which becomes much weaker after the diyne polycyclotrimerization reaction. The C≡C stretching vibration at 2107 cm^{-1} is hardly discernible, indicating that a large portion of the acetylene triple bonds of the molecules of the diyne monomer have been consumed by the polymerization reaction, with only a small portion of the triple bonds left intact, existing as the linear and terminal units in the polymer structure (cf., Chart 2).

Similar results are obtained from the NMR analyses. Figure 2 shows the ^{1}H NMR spectra of *hb*-P**1**(6) and its monomer **1**(6) in DCM-d_2. The acetylene protons of **1**(6) resonate at δ 3.07, whose intensity becomes much lower in the spectrum of *hb*-P**1**(6). Most of these unreacted acetylenic triple bonds exist as end groups on the peripheries of the polymer, offering an opportunity to decorate the macromolecule with other functional groups by end-capping reactions. Additionally, new resonance peaks are emerged in the aromatic region and the "old" peaks at δ 7.2−6.8 and

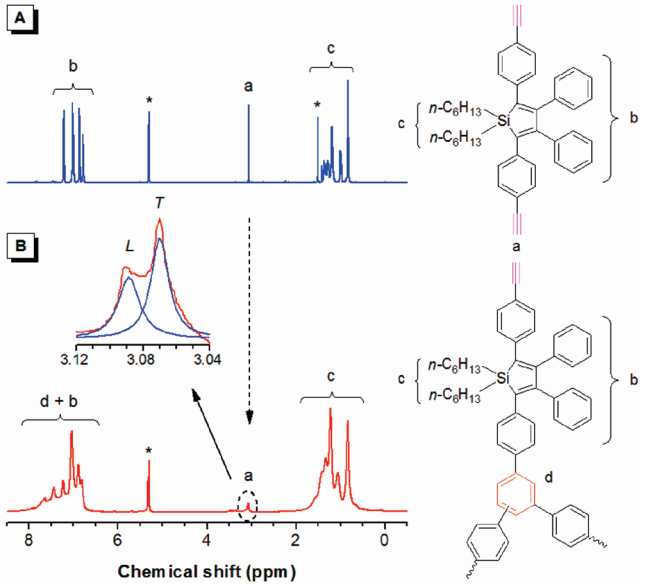

Figure 2. ^{1}H NMR spectra of DCM-d_2 solutions of (A) monomer **1**(6) and (B) its polymer *hb*-P**1**(6) (sample taken from Table 1, no. 3). Inset in panel B: resolved peaks for the resonances of the acetylenic protons. The solvent peaks are marked with asterisks.

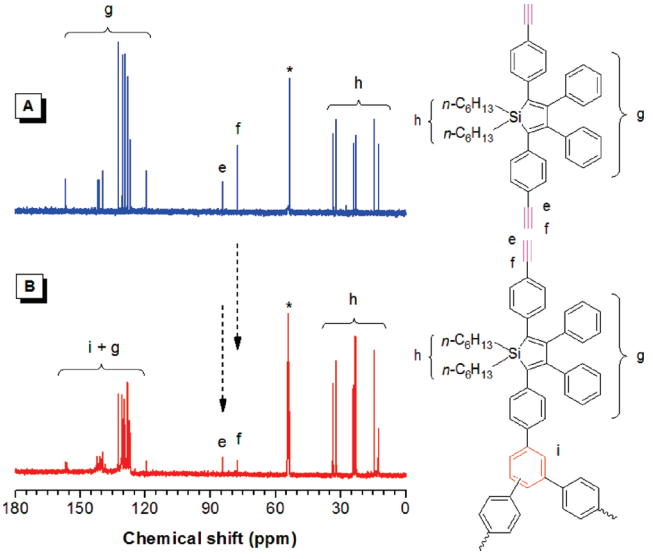

Figure 3. ^{13}C NMR spectra of DCM-d_2 solutions of (A) monomer **1**(6) and (B) its polymer *hb*-P**1**(6) (sample taken from Table 1, no. 3). The solvent peaks are marked with asterisks.

1.5−0.8 are greatly broadened after the polymerization reaction. All these spectral data indicate that the acetylenic triple bonds of monomer **1**(6) have been cyclotrimerized to form benzene rings in polymer *hb*-P**1**(6). From our previous results on the cyclotrimerization of phenylacetylene as a model reaction,[13] the new resonance peaks correspond to the absorption of the protons on the newly formed 1,2,4- and 1,3,5-trisubstituted benzene rings.

Similarly, ^{13}C NMR spectrum of *hb*-P**1**(6) shows weak resonance peaks of acetylenic carbon atoms at δ 84.3 and 77.5 and new resonance peaks of aromatic carbon atoms in the downfield region (Figure 3). All the resonance peaks in both the ^{1}H and ^{13}C NMR spectra can be readily identified and assigned without difficulty, as marked in Figures 2 and 3. No any strange peaks are observed, indicative of the high purify of the isolated polymer products. The IR and

NMR spectra exemplified here and the spectral data given in the Experimental Section duly confirm that silole monomers **1**(*m*) have undergone the diyne polycyclotrimerization reactions to yield hyperbranched polysiloles *hb*-**P1**(*m*) with expected structures (cf., Scheme 1).

Determination of Degree of Branching (DB). From the ^{1}H NMR spectra shown in Figure 2, the extent of conversion (p) of the acetylenic triple bonds that have been transformed to benzene rings can be estimated using eq 1:

$$p = \frac{N_{RT}}{N_{TT}} = \frac{A_{Ph} - \frac{A_{alkyl}}{4m+2} \times 18}{\frac{A_{alkyl}}{4m+2} \times 2} = \frac{(2m+1)A_{Ph} - 9A_{alkyl}}{A_{alkyl}} \quad (1)$$

where N_{RT} is the number of the reacted triple bonds, N_{TT} is the total number of the triple bonds of the monomers, A_{Ph} is the integrated area of the resonance peaks for the protons of all benzene rings in the polymer, A_{alkyl} is the integral of the aliphatic resonance peaks, and m is the number of the carbon atoms in the alkyl chain (m = 1, 6) attached to the silicon atom at the 1,1-positions in the silole ring.

Generally speaking, the polycyclotrimerization reaction should be terminated before the critical extent of conversion (p_c) or gel point in order to obtain a soluble polymer. In our previous study, from a pure structure point of view, we have theoretically derived that if no loops are formed in the propagation step of the diyne polycyclotrimerization, the upper limit of the p value is equal to 75%.[13] On the basis of a kinetic model, Malkov et al. have performed the theoretical studies of polycyclotrimerization and predicted p_c values of 0.50 and ~0.62 with nonallowance and allowance for the first shell negative substitution effect, respectively.[20] The monomer solution we normally used for the polymerization is so dilute that it will result in a high p_c value (>0.62). Indeed, the p value of *hb*-**P1**(6) prepared under the conditions shown in Table 1, no. 3 is theoretically predicted to be 73.8%. We believe that when the p value is less than 75%, the probability of loop formation is very low. To simplify the structural analysis, we assume that no loop structures are formed in the polymer at p < 75%. On the basis of this hypothesis, we have established the relationships between p and the number of newly formed benzene rings (N_b) and between the degree of polymerization (DP_n) and N_b:[13]

$$p = \frac{3N_b}{4N_b + 2} \quad (2)$$

$$DP_n = 2N_b + 1 \quad (3)$$

Since p equals to 0.738, the values of N_b and DP_n are calculated to be 30.8 and 62.6, respectively. Thus, the number-average MW of the polymer (M_n) can be derived by eq 4:

$$M_n = DP_n \times M_m = 37700 \quad (4)$$

where M_m is the MW of monomer **1**(6). Comparing the calculated M_n value with that estimated by GPC relative to the polystyrene standards, the difference is found to be as large as about 6 times because of the globular architecture of the hyperbranched polymer:

$$\frac{M_{n(NMR)}}{M_{n(GPC)}} = \frac{37700}{6700} = 5.63 \quad (5)$$

For the polycyclotrimerization of an A_2-type diyne monomer, if p < 75% and no loop is formed, eqs 6 and 7 hold:[13]

$$\frac{2f_T + f_L}{f_T - f_D} = DP_n(1-p) \quad (6)$$

$$f_T + f_D + f_L = 1 \quad (7)$$

where f_D, f_T, and f_L are the fractions of dendritic (D), terminal (T) and linear (L) units, respectively (Chart 2). Because of the difficulty in differentiating the newly formed benzene rings in the D, T, and L units from each other by the spectroscopic techniques, we diverted our effort to analyze the acetylenic proton signal. Magnification of the proton signal at δ 3.07 reveals that it is actually comprised of two peaks (cf., Figure 2). We assigned the sharper peak to the resonance of protons of the peripheral T units because of the faster exchange caused by their more rapid molecular motion in comparison to that of the L units, which are embedded in the hyperbranched sphere. Fitting the two peaks gives the result that the amount of the acetylenic protons in the T units is ~1.34-fold higher than that in the L units. Because there are two such protons in the T unit but only one in the L unit, eq 8 can be established:

$$\frac{2f_T}{f_L} = \frac{A_T}{A_L} = 1.34 \quad (8)$$

where A_T and A_L are the integrated areas of the resonance peaks for the protons of the T and L units, respectively. By combining eqs 6−8, the values of f_D, f_T and f_L are calculated to be 0.24, 0.31 and 0.45, respectively. According to definition, DB is expressed as:[21]

$$DB = \frac{f_D + f_T}{f_D + f_T + f_L} = 1 - f_L = 0.55 \quad (9)$$

The DB value of our polymer (0.55) is comparable to the most probable DB values for the conventional hyperbranched polymers prepared by the condensation polymerization of AB_2-type monomers (~0.5).[22] This further confirms the hyperbranched topological structure of our polymer.

Thermal Properties. Thermal stabilities of *hb*-**P1**(*m*) were evaluated by thermogravimetric analysis (TGA). Polymer *hb*-**P1**(1) is thermally stable and loses 5% of its original weight when it is heated to a temperature of about 370 °C (Figure 4). More than 75% of its weight is still retained even when the temperature is raised to as high as 500 °C. Similar thermal properties are observed in the case of *hb*-**P1**(6). The high thermal stabilities of *hb*-**P1**(*m*) are in some sense expected because the hyperbranched polymers are basically comprised of stable aromatic rings with high resistance to thermolytic attacks. The thermally induced cross-linking of the acetylenic triple bonds may have also contributed to the high thermal stabilities of the polymers.[23]

To examine whether the hyperbranched polymers are indeed thermally curable, we used differential scanning calorimetry (DSC) to follow their thermal transitions. In the first heating scan, a very broad exothermic peak starts to

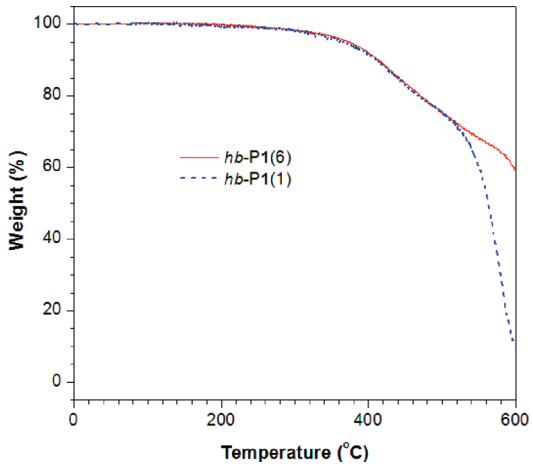

Figure 4. TGA thermograms of *hb*-P**1**(1) (sample taken from Table 1, no. 2) and *hb*-P**1**(6) (Table 1, no. 3) recorded under nitrogen at a heating rate of 10 °C/min.

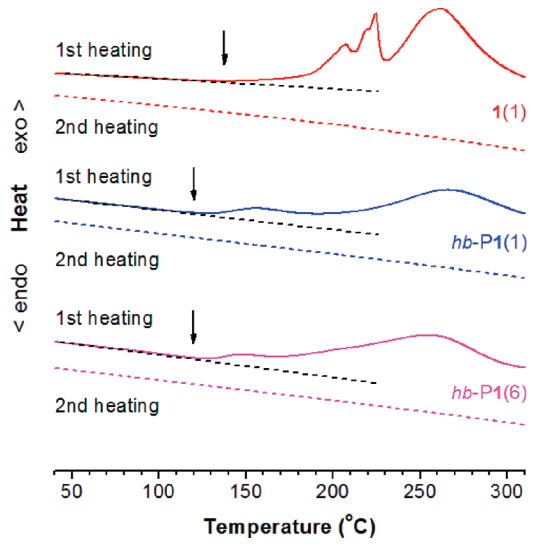

Figure 5. DSC thermograms of **1**(1) and *hb*-P**1**(*m*) (samples taken from Table 1, nos. 2 and 3) measured at a scan rate 10 °C/min under nitrogen.

emerge from ~120 °C in the thermogram of *hb*-P**1**(1) (Figure 5). Since the polymer does not loss its weight below 370 °C, the exothermic peak at ~267 °C is thus not due to the chain scission but associated with the thermally induced alkyne polymerization.[23] The second heating scan of the DSC analysis gives an even line in the same temperature region, suggesting that all the acetylenic triple bonds have reacted during the first heating scan. A similar thermogram is obtained for *hb*-P**1**(6) and the cross-linking reaction also starts from ~120 °C with an exothermic peak at ~256 °C.

If the thermal curing of the hyperbranched polymers is really associated with the thermal cross-linking of their triple-bond functional groups, their monomers should also be thermally polymerizable. This is indeed the case. As can be seen from the DSC thermogram of **1**(1) shown in Figure 5, its thermal curing commences from ~130 °C. The thermogram recorded during the first cycle is featured with a series of continuous exothermal peaks at 208, 218, 225, and 262 °C with the last peak being the broadest. The spectral profile generally resembles those of the polymers, suggestive of occurrence of the same reaction. Similarly, no thermal transition peaks are recorded during the second heating scan.

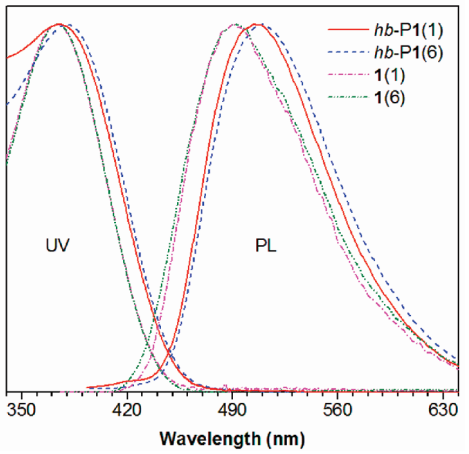

Figure 6. Normalized UV and PL spectra of THF solutions of **1**(*m*) and *hb*-P**1**(*m*). Concentration: 10 μM. Excitation wavelength: 373 nm.

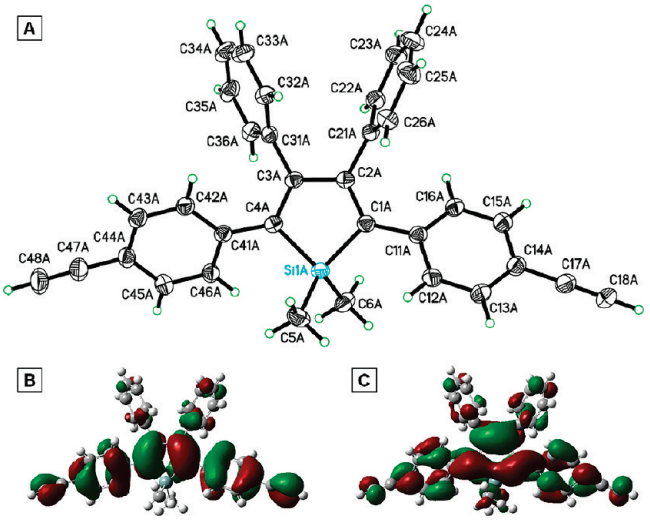

Figure 7. (A) ORTEP drawing of crystal structure of **1**(1) and molecular orbital amplitude plots of its (B) HOMO and (C) LUMO.

Photophysical Properties. Figure 6 shows the UV and PL spectra of **1**(*m*) and their polymers in THF solutions. The absorption spectrum of *hb*-P**1**(1) is peaked at 379 nm, while the absorption maximum of **1**(1) is located at 373 nm. Similarly, the absorption peak of *hb*-P**1**(6) is 7 nm bathochromically shifted from that of **1**(6). Upon photoexcitation, *hb*-P**1**(1) and *hb*-P**1**(6) emit green lights of 507 and 509 nm, respectively, while the PL spectra of their monomers are peaked at a shorter wavelength of ~490 nm. All the absorption and emission data indicate a more extended electronic conjugation in the polymer system. Evidently, the hookup of the silole rings by the benzene rings formed in the cyclotrimerization polymerization at the 2,5-positions in three-dimensional space has helped increase the effective length of electronic conjugation.

To prove that the electronic conjugation in a silole molecule is affected by the substituents at the 2,5-positions,[6g,24] we carried out theoretical calculation based on the density functional theory (DFT) at the B3LYP/6-31G* level.[25] The molecular geometry of monomer **1**(1) used in the calculation is extracted from its single crystal structure (Figure 7). The HOMO and LUMO of the isolated single molecule of **1**(1) are mainly localized in the silacyclopentadiene ring and the two ethynylphenyl groups at the 2,5-positions.[16f,24] This verifies that the 2,5-aryl groups have a strong influence on

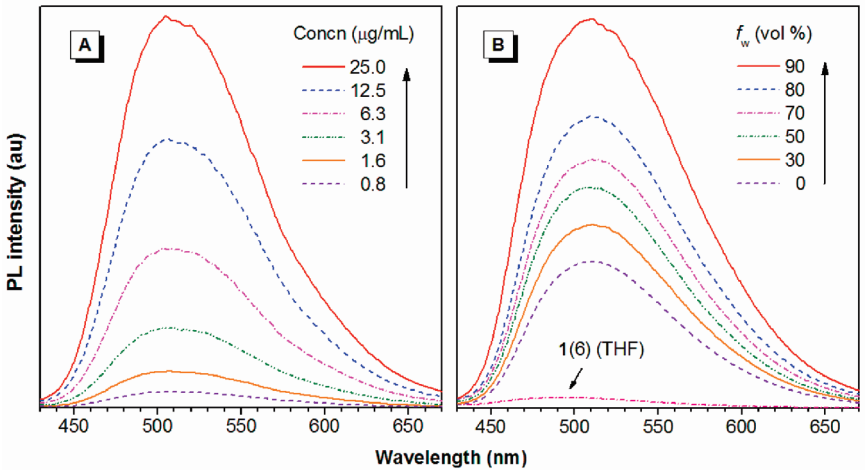

Figure 8. (A) Concentration-dependent PL spectra of *hb*-P**1**(6) in THF solutions. (B) PL spectra of *hb*-P**1**(6) in THF/water mixtures with different water fractions (f_w). PL spectrum of **1**(6) in THF is shown for comparison. Concentration: 10 μM; excitation wavelength: 373 nm.

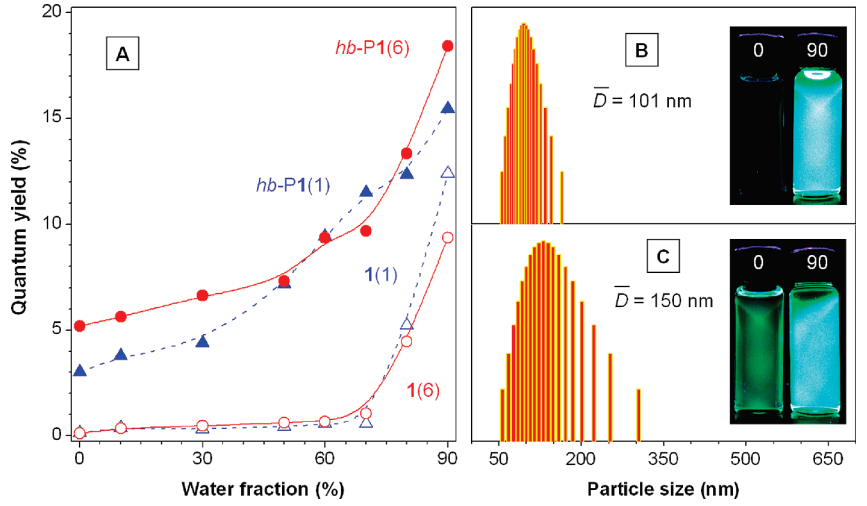

Figure 9. (A) Variations in quantum yields of **1**(*m*) and *hb*-P**1**(*m*) with water fractions (f_w) in THF/water mixtures. Size distributions of nanoaggregates of (B) **1**(6) and (C) *hb*-P**1**(6) in a THF/water mixture with f_w = 90%. Concentration: 10 μg/mL. Insets: fluorescent images of (B) **1**(6) and (C) *hb*-P**1**(6) taken under UV illumination in pure THF (f_w = 0) and a THF/water mixture with f_w = 90%.

the energy band gap of a silole molecule. Clearly, the electronic conjugation is extended when **1**(1) is transformed to *hb*-P**1**(1), in which the silole rings are connected by the new benzene rings at the 2,5-positions.

We have proposed the RIR process as the main cause for the AIE effect of siloles.[3−5] Fundamental physics teaches us that any molecular motions consume energy. The peripheral phenyl rings (rotors) surrounding the silole core (stator) can rotate via the single-bond axes. In the solution state, the active intramolecular rotation serves as a relaxation channel for the excited state to decay, hence rendering the silole molecules nonemissive. In the aggregated state, however, such rotation is physically restricted, which blocks the nonradiative pathway and populates the radiative excitons, thus enabling the molecules to luminesce efficiently. Monomers **1**(1) and **1**(6) are AIE luminogens and emit weakly in the dilute solutions of their good solvents (e.g., THF; Figure 8B). Their hyperbranched polymers, however, are somewhat luminescent in their THF solutions, as exemplified by the fluorescent image of the *hb*-P**1**(6) solution shown in Figure 9C. The silole units are located within the stiff polymer spheres, which limit their intramolecular rotations to some extent and thus render the polymers somewhat luminescent in the solution state.

Light emission of conjugated polymers often suffers from concentration-quenching or ACQ effect due to the formation of nonradiative species such as excimers and exciplexes, which significantly limits the scope of their technological applications, especially in optoelectronic devices. In sharp contrast, our hyperbranched polymers emit strongly upon aggregation. As shown in Figure 8A, the PL of *hb*-P**1**(6) is progressively intensified when its solution is thickened from 0.8 to 25 μg/mL. Addition of a nonsolvent such as water into THF induces the molecules of *hb*-P**1**(6) to aggregate and enhances its PL (Figure 8B). The higher is the water fraction, the stronger is the light emission. Evidently, the emission of *hb*-P**1**(6) is enhanced by aggregate formation; in other words, the polymer shows a typical effect of AEE.

The mechanism for the AEE effect is similar to that for the AIE system discussed above. Comparative studies of the photophysical properties of the AIE-active monomers and their AEE-active polymers from molecular solutions in their good solvents to nanoparticle suspensions in their poor solvents and to thin films in the solid state may help gain further insights into the novel phenomena. The absorption spectra of the monomer aggregates in THF/water mixtures with 90 vol % water fraction are almost the same as those of

Table 2. Absorption and Emission Properties of Monomers and Their Polymers in Solution (soln),[a] Aggregate (aggr),[b] Film,[c] Crystalline (cryst), and Amorphous (amor) States

	λ_{ab} (nm)[d]		λ_{em} (nm)[e]					Φ_F (%)[f]		
	soln	aggr	soln	aggr	film	cryst	amor	soln	aggr	α_{AIE}[g]
1(1)	373	371	490	492	484	494	507	0.1	12.4	124.0
hb-**P1**(1)	379		507	508	489		523[h]	3.0	15.4 (25.6)	5.1
1(6)	373	372	491	497	480		507[i]	0.1	9.4	94.0
hb-**P1**(6)	380		509	510	490		526[h]	5.2	18.4 (23.3)	3.5

[a] In THF solution (10 μM). [b] In THF/water (10:90 v/v) mixture (10 μM). [c] Prepared by spin-coating a 1,2-dichloroethane solution of a pure polymer or a blend of monomer (2.5 wt %) and poly(methyl methacrylate) (PMMA). [d] Absorption maximum. [e] Emission maximum. [f] Fluorescence quantum yield estimated using 9,10-diphenylanthrance as standard (Φ_F = 90% in cyclohexane). Given in the parentheses is the absolute Φ_F value in the solid state determined by a calibrated integrating sphere. [g] AIE factor defined by eq 10. [h] Prepared by static casting of a polymer solution. [i] Viscous liquid.

their THF solutions. The spectra of the polymer aggregates resemble those of their solid thin films and covered a wide spectral region with no clearly discernible peaks (Supporting Information, Figure S2). In THF, the fluorescence quantum yield (Φ_F) of **1**(*m*) is 0.1%, whereas *hb*-**P1**(1) and *hb*-**P1**(6) show relatively higher values of 3.0% and 5.4%, respectively (Table 2). The Φ_F values of **1**(*m*) remain unchanged until ~70 vol % water is added into THF (Figure 9A). Afterward, the fluorescence efficiencies rise swiftly.

The Φ_F values of the hyperbranched polymers, on the other hand, are monotonically increased with an increase in the water content (Figure 9A). In comparison to their monomers, the polymers are more sensitive in morphology to the change in their surrounding environments. Even when a small amount of water is added into THF, the subtle change in the solvating power of the solvent mixture can be sensed by the macromolecules, causing them to aggregate. At the same water contents, the Φ_F values of the polymers are always higher than those of their monomers. This may be explained by the fact that the motions of **1**(*m*) are only restricted by physical aggregation, whereas both internal and external factors of chemical binding and physical aggregation are involved in the RIR processes of the polymers.

In the THF/water mixtures with 90 vol % water fraction, the Φ_F values of **1**(1) and **1**(6) are 12.4% and 9.4%, respectively, giving the corresponding α_{AIE} values of 124 and 94 (Table 2), where α_{AIE} is the AIE factor defined by the following eq:[26]

$$\alpha_{AIE} = \frac{\Phi_{F(aggr)}}{\Phi_{F(soln)}} \tag{10}$$

The Φ_F values of *hb*-**P1**(1) and *hb*-**P1**(6) in the same solvent mixture are 15.4% and 18.4%, respectively, which are 3.5−5.1 times higher than those in the THF solutions. The fluorescence images shown in panels B and C of Figure 9 visually demonstrate the AIE and AEE phenomena of **1**(6) and *hb*-**P1**(6), respectively. Particle size analyses reveal the existence of particles with average sizes of 101 and 150 nm in the solvent mixture with 90 vol % water content for **1**(6) and *hb*-**P1**(6), respectively. The AEE effect enables the polymers to emit efficiently in the solid state. The absolute Φ_F values of the thin solid films of *hb*-**P1**(1) and *hb*-**P1**(6) measured by an integrating sphere are as high as 25.6% and 23.3%, respectively (Table 2).

Fluorescence Decay Dynamics. Lifetime is an important kinetic parameter for the PL decay process. Study of emission dynamics of the monomers and their polymers by time-resolved technique may help deepen our understanding on the AIE and AEE mechanisms. Figure 10 shows the PL decay curves of **1**(6) and *hb*-**P1**(6) in THF solutions as examples. The PL of monomer **1**(6) decays faster than that of its polymer *hb*-**P1**(6). The excited state of **1**(6) decays in a single-exponential fashion with a lifetime as short as ~90 ps (Table 3), suggesting that all the excited molecules relax

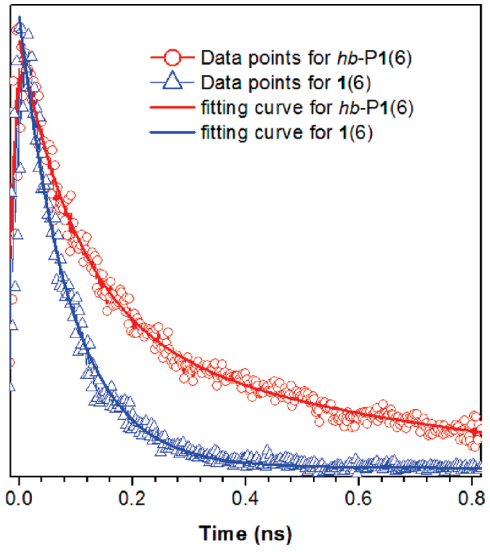

Figure 10. Fluorescence decay curves of THF solutions (1 μg/mL) of **1**(6) and *hb*-**P1**(6).

Table 3. Fluorescence Decay Parameters of 1(*m*) and *hb*-P1(*m*) in Dilute THF Solutions[a]

	A_1 (%)	A_2 (%)	τ_1 (ns)	τ_2 (ns)	$\langle\tau\rangle$ (ns)
1(1)	100	0	0.05		0.05
hb-**P1**(1)	73	27	0.09	0.82	0.29
1(6)	100	0	0.09		0.09
hb-**P1**(6)	62	38	0.10	0.66	0.31

[a] The dynamic parameters (A_i, τ_i, and $\langle\tau\rangle$) were calculated from eqs 20 and 21; see Experimental Section for details.

through the same pathway. The decay curve of *hb*-**P1**(6), on the other hand, is better fitted by a double-exponential function. This means that two relaxation pathways are involved in its decay process: 62% (A_1) and 38% (A_2) of the excitons decay via the fast and slow channels with lifetimes of 0.10 ns (τ_1) and 0.66 ns (τ_2), respectively.

The Φ_F value is known to be associated with the fluorescence lifetime by the following eq

$$\Phi_F = \frac{\tau}{\tau_r} \tag{11}$$

where τ is related to radiative (τ_r) and nonradiative (τ_{nr}) lifetimes by the expressions of

$$\frac{1}{\tau} = \frac{1}{\tau_r} + \frac{1}{\tau_{nr}} \tag{12}$$

$$k = k_r + k_{nr} \tag{13}$$

where k_r and k_{nr} are the radiative and nonradiative decay rates, respectively.[1,27] The τ_r term is an intrinsic property of a

molecule. Consequently, the faster is the nonradiative decay rate (k_{nr}), the lower is the Φ_F value. The short-lived excited state and the low Φ_F value of **1**(6) in the THF solution indicate that there exist vigorous nonradiative paths leading to effective quenching of its PL in the dilute solution. Rotational energy relaxations are known to nonradiatively deactivate the excited states. In the molecular solution of **1**(6), the intramolecular rotations are active and the excited states of the monomer molecules are readily annihilated through the nonradiative deactivation process. However, in the solution of *hb*-**P1**(6), the probability of intramolecular rotations of the phenyl rotors in the silole units is decreased due to the polymer effect discussed above, which partially blocks the nonradiative relaxation channel. Thus, both the emission lifetime and efficiency of the polymer in the solution are enhanced. Similar behaviors are observed in the **1**(1)/*hb*-**P1**(1) pair (Table 2). These results strongly support the validity of the RIR model for the AIE and AEE effects.

Solid-State Emissions. After studying the emissions of **1**(*m*) and *hb*-**P1**(*m*) in the molecular solutions in good solvents and the nanoparticle suspensions in poor solvents, we investigated their PL behaviors in the condensed phase. Both the monomers and polymers show strong solid-state emissions, as can be seen from the examples of fluorescence images shown in Figure 11. The crystals of **1**(1) emit at 494 nm, which is blue-shifted from that of its amorphous powder by 13 nm (Figure 12). Crystallization generally red-shifts

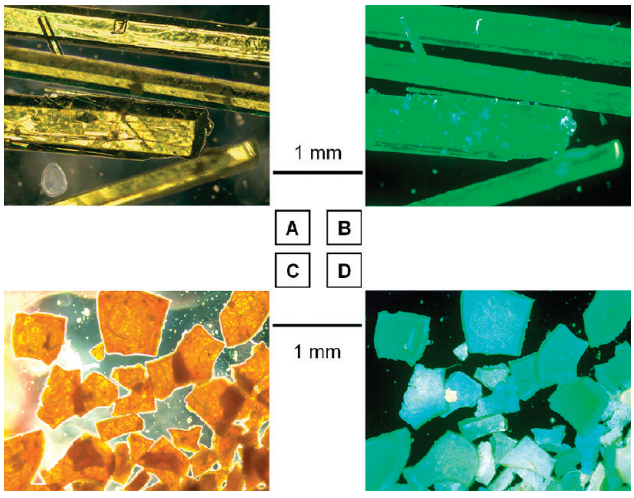

Figure 11. Photographs of (A and B) crystalline rods of **1**(1) and (C and D) amorphous plates of *hb*-**P1**(6) taken under (A and C) normal laboratory lighting and (B and D) UV illumination (330−380 nm).

fluorescence, but why is the opposite effect observed in **1**(1)? Scrutinization of the molecular conformation and packing arrangement of **1**(1) in the crystalline phase offers some clue.[3,28] As shown in Figure 7A, the molecule of **1**(1) takes a propeller-shaped conformation in the crystalline state. The peripheral phenyl rings are twisted out of the silacyclopentadiene plane to varying extents, with dihedral angels of ~21° and ~37° for the phenyl rotors at the 2,5-positions and larger twists of ~52° and ~57° at the 3,4-positions. The sp^3 hybridization of the silicon atom makes the 1,1-methyl groups completely out of plane of the silole core. The nonplanarity caused by the steric repulsion between the phenyl groups and the sp^3 hybridization of the silicon atom reduces the intermolecular interactions and the likelihood of excimer formation. The physical confinement in the crystal lattice rigidifies the conformation of the molecules of **1**(1), thereby enabling it to emit efficiently in the solid state.

The unusual blue shift observed in the crystalline phase is attributable to the conformational twisting in the molecular packing process, during which the molecules of **1**(1) adjust their conformations in order to fit into crystalline lattice (Figure 13). The twisted conformation is stabilized by the C−H···π hydrogen bonds (d_1 = 2.721 Å) between the hydrogen atom in a phenyl group in one silole molecule and the π electron cloud of a phenyl ring in another neighboring molecule. Without these physical restraints, the silole molecules in the amorphous powder may statistically assume a more planar conformation and thus show a redder emission. The large intermolecular distances (d_2 = 7.346 Å, d_3 = 7.760 Å, and d_4 = 12.140 Å) in the crystal packing structure manifest the lack of strong chromophore interactions that tend to induce nonradiative transitions and red shifts as seen in the conventional luminophore crystals with strong $\pi-\pi$ stacking interactions. Additionally or alternatively, the conformation rigidification enforced by the crystal packing of AIE luminogen molecules hampers vibrational relaxations and favors vertical transitions, according to the Franck−Condon principle. The bigger energy gap involved in the vertical transition thus leads to the bluer emission in the crystalline state.

Since the conformations of silole molecules can affect their photophysical processes, it is envisioned that if a method for conformational alteration can be developed, the similar morphochromism should be observed. We prepared blend films by spin-coating the solutions of **1**(1)/PMMA mixtures onto silicon wafers. The idea is that at a low doping concentration, the molecules of **1**(1) should be well isolated or segregated in the dense polymer matrix. The shearing effect of the spin-coating process may force the silole molecules to

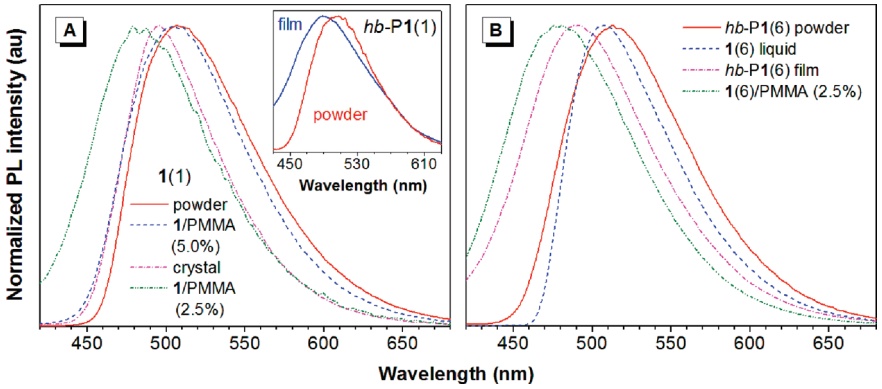

Figure 12. (A) PL spectra of **1**(1) dispersed in PMMA films and in powdery and crystalline states. Inset: PL spectra of spin-coated film and amorphous powder of *hb*-**P1**(1). (B) PL spectra of viscous liquid of **1**(6), spin-coated film of **1**(6)/PMMA, and spin-coated film and amorphous powder of *hb*-**P1**(6).

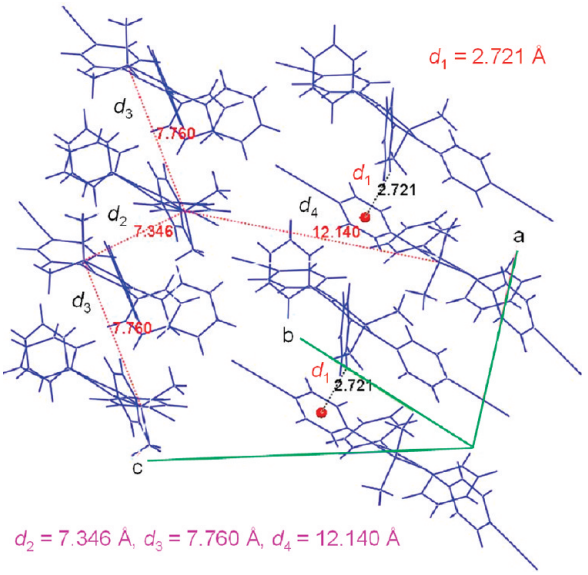

Figure 13. Perspective view of packing arrangements in the crystals of **1**(1), with C−H···π hydrogen-bonding (d = 2.721 Å) and other intermolecular distances marked by dashed lines.

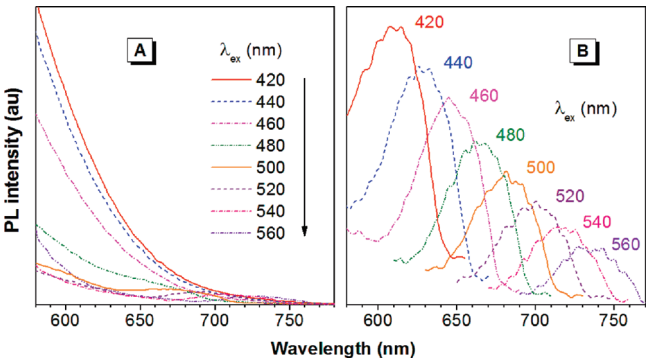

Figure 14. Excitation wavelength (λ_{ex})-dependent PL spectra of *hb*-P**1**(6) (sample taken from Table 1, no. 3) (A) before and (B) after thermal curing at 400 °C for 1 min.

take a more twisted conformation and thus emit a bluer light. As anticipated, the PMMA film containing 2.5 wt % of **1**(1) shows an emission maximum at 484 nm, which is 10 nm bluer than the crystal emission. When the doping concentration is increased to 5 wt %, the emission peak is red-shifted to 505 nm. At the high doping concentration, the silole molecules may cluster together, in which free volumes are created due to the large intermolecular distances. This allows the molecules to structurally relax to comparatively more planar conformations, thereby red-shifting the emission peak. Similarly, a blue shift of 27 nm is observed in monomer **1**(6) when 2.5 wt % of its viscous liquid is doped into the PMMA matrix (Figure 12B).

We further investigated the PL behaviors of the hyperbranched polymers. It is noteworthy that the light emissions of the thin films of the polymers spin-coated from their 1,2-dichloroethane solutions are hypsochromically shifted from those of their amorphous powders by 34−36 nm, as can be seen from the examples of PL spectra of *hb*-P**1**(1) shown in the inset of Figure 12A and the emission data summarized in Table 2. It can be rationalized that the shearing force in the spin-coating process has helped populate the emitting species in the polymers with more twisted molecular conformations that have been instantly frozen in the dense matrices due to

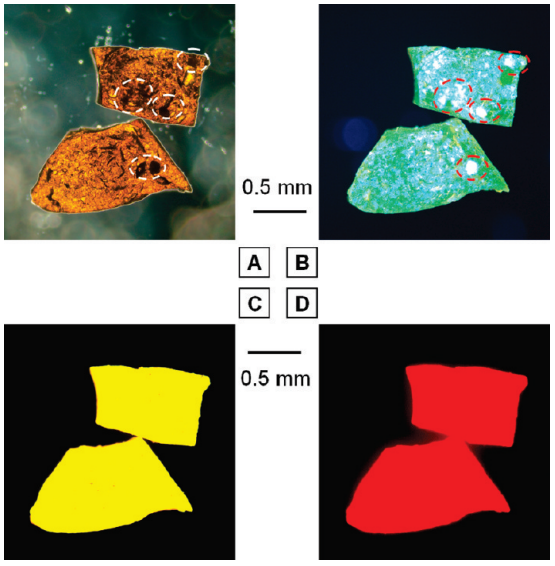

Figure 15. Photographs of thermal curing product of *hb*-P**1**(6) taken (A) under normal room lighting and upon excitation with (B) UV (330−380 nm), (C) blue (450−490 nm), and (D) green (510−560 nm) lights.

the rapid evaporation of the solvent and the quick formation of the glassy film.

Fluorescent Modulation and Photopatterning. The DSC analyses reveal that **1**(*m*) and *hb*-P**1**(*m*) can be thermally cured and our previous studies have found that diynes and their polymers prepared by polycyclotrimerization are photocross-linkable (Scheme 2).[9] The IR spectra of **1**(1) after thermolysis and photolysis show absorption bands in the olefinic region of 1690−1600 cm^{-1} (Supporting Information, Figure S3), suggesting that the triple bonds of **1**(1) have been transformed into double bonds of polyenes and that the effective conjugation of *hb*-P**1**(*m*) can be lengthened by the curing reaction. Indeed, the thermally cross-linked product of *hb*-P**1**(6), abbreviated as X-*hb*-P**1**(6), emits in the red spectral region (Figure 14). Remarkably, the PL spectrum of X-*hb*-P**1**(6) is sensitive to the excitation wavelength, which is not observed in its precursor *hb*-P**1**(6). The emission peak is gradually red-shifted from 610 to 735 nm accompanying with a decrease in the emission intensity when the excitation wavelength is changed from 420 to 560 nm at an interval of 20 nm (Figure 14B). This fact evinces that the curing product possesses various conjugation lengths with different populations, which response to the matched stimuli. This enables the cross-linked polymer to emit lights of different colors in response to the variations in the excitation wavelengths.

After thermal curing, the orange appearance of *hb*-P**1**(6) changes to brown, with some parts becoming even dark, as circled by the dotted lines in Figure 15A. The dark areas may be rich in the polyene structure that can absorb lights of long wavelengths. Under the illuminations of UV, blue and green lights, X-*hb*-P**1**(6) shows green, yellow and red emissions, respectively (Figure 15, panels B−D), which are consistent with the PL spectral data discussed above. From these results, it can be concluded that various conjugation lengths or band gaps exist in X-*hb*-P**1**(6). Notably, many white light-emitting dots are observed under the UV light illumination (Figure 15B). When irradiated by the UV light, polymer branches with appropriate conjugation lengths will be pumped to their excited states and emit blue to green lights, which can serve as excitation sources to induce yellow and

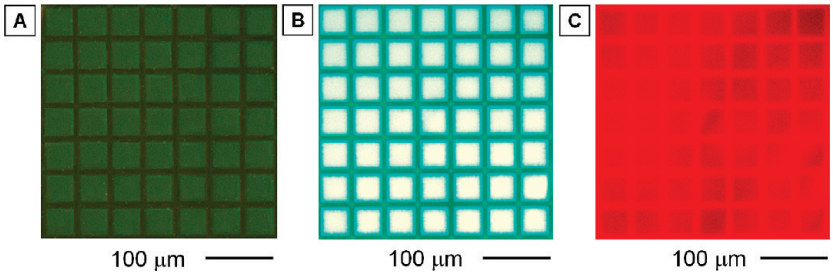

Figure 16. Two-dimensional photopatterns generated by UV irradiation of *hb*-**P1**(6) (sample taken from Table 1, no. 3). Photographs were taken by fluorescence microscopy (A) under normal laboratory lighting and upon excitations with (B) UV (330−380 nm) and (C) green (510−560 nm) lights.

red emissions from the branches with longer conjugations. Admixture of these emitted lights results in the emission of a white light. It is envisioned that specific areas of a film of the polymer can be cured or cross-linked by local heating with laser or electron beam to modulate the band gap and hence to obtain fluorescence patterns with different emission colors, which may find an array of applications in information storage and multicolor imaging or display systems.

Light-driven technique is more convenient, in terms of operational simplicity and precise control of curing reaction and patterning process. Because our polymers possess good film-forming ability and are photosensitive and light-emitting, they are promising candidates for fabrication of luminescent patterns by photolithography process. Creations of fluorescent patterns is of great importance to the construction of photonic and electronic devices and to the development of biological sensing and probing systems, such as OLED, liquid-crystal display, and medicinal diagnostic biochip.[29] When a thin spin-coated film of *hb*-**P1**(6) is irradiated by a UV light for 20 min through a copper negative mask, the exposed region of the film is rendered cross-linked and hence insoluble.[13,14] A two-dimensional photopattern is generated without development. The good quality of the pattern (sharp line edges, uniform film thickness, etc.) is clearly seen under normal laboratory lighting (Figure 16A), although the photolysis process is yet to be optimized. Since the effective conjugation of *hb*-**P1**(6) can be lengthened by a cross-linking reaction, the exposed and unexposed areas of the film are expected to show different emission behaviors. To verify this, the PL spectra of the thin solid film of X-*hb*-**P1**(6) are taken (Supporting Information, Figure S4). Indeed, the polymer film shows excitation wavelength-dependent emission peaks with spectral profiles similar to those of the thermal curing product (cf., Figure 14).

The unexposed squares of the patterned film emit intense green light, which is so bright that it looks white visually, under UV illumination (Figure 16B). This emission corresponds to the inherent energy band gap of *hb*-**P1**(6). The exposed cross-linked lines, however, show only faint emission, probably due to the mismatching with the excitation wavelength, coupled with the oxidation during the patterning process performed in air (Supporting Information, Figure S3). On the contrary, when excited by a green light, the exposed areas or the patterned lines emit a red light (Figure 16C), whereas the unexposed areas are almost nonemissive, owing to their weak absorption in the green spectral region. Evidently, the emission colors of our polymers are readily tuned by the photoinduced curing reaction. The multicolor light-emitting patterning of the polymers may allow them to be used in the constructions of wavelength-dependent and -manipulable optical and photonic devices. This exciting possibility is currently under active exploration in our laboratories.

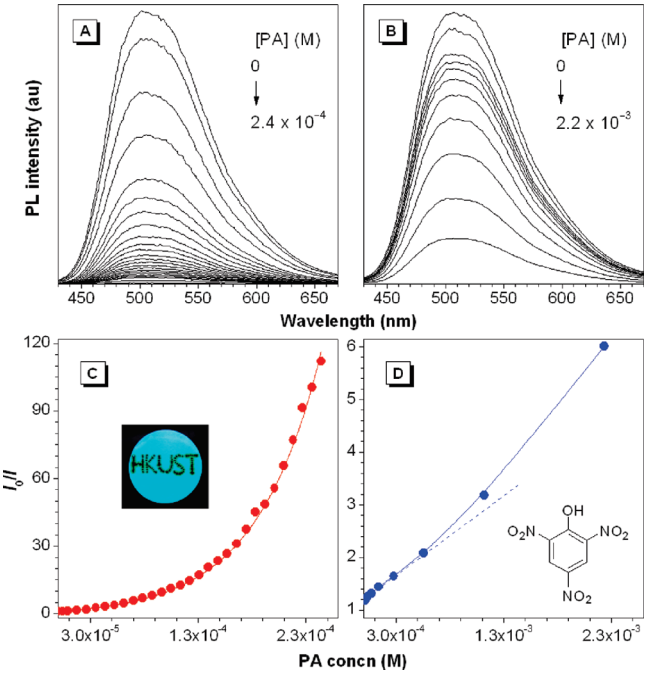

Figure 17. PL spectra of *hb*-**P1**(6) in (A) THF/water mixture (1:9 v/v) and (B) THF containing different amounts of picric acid ([PA]). Polymer concentration: 0.17 μM. Plots of I_0/I vs [PA] in (C) THF/water mixture (1:9 v/v) and (D) THF. Inset of panel C: fluorescence image of *hb*-**P1**(6) deposited on a filter paper. The letters "HKUST" were written by dropping aliquots of a PA solution on the filter paper using a capillary tube. Inset in panel D: chemical structure of PA.

Superamplified Explosive Detection. Nitroaromatic compounds such as 2,4-dinitrotoluene (DNT), 2,4,6-trinitrotoluene (TNT), and picric acid (PA) are warfare explosives, sensitive detection of which is of antiterrorism implications. In recent years, the detection of explosives using fluorescent probes based on conjugated polymers has attracted much interest.[30,31] Our hyperbranched polymers have the following unique features: (i) extended electronic conjugation with AEE activity and signal-amplifying effect,[8,11,30,31] (ii) high binding capability to analytes due to the presence of numerous molecular cavities and the potential involvement of Lewis acid−base interactions,[30−32] and (iii) multidimensional excitonic migration pathways in the three-dimensional space.[30] It is thus expected that *hb*-**P1**(*m*) may function as sensitive fluorescent chemosensors for explosive detection. Because of its commercial availability, we used PA as a model explosive in this work. The nanoaggregates of *hb*-**P1**(6) in the THF/water mixture with 90 vol % water were employed as the fluorescent sensor, while its isolated molecules in pure THF solution was studied for comparison.

With gradual addition of PA to the nanoparticle suspension of *hb*-**P1**(6) in the aqueous mixture, the emission intensity of

the polymer aggregates is progressively decreased, while the PL spectral profile maintains unchanged (Figure 17A). The PL quenching can be clearly recognized at a PA concentration as low as 1 μg/mL or 1 ppm. Remarkably, the Stern−Volmer plot of I_0/I versus [PA] shows a upward bent curve instead of a linear line (Figure 17C). The PL of *hb*-**P1**(6) in the THF solution also becomes weaker in the presence of PA. Its corresponding Stern−Volmer plot also bends upward (Figure 17D). At a PA concentration of 2.4×10^{-4} M, the PL intensity of *hb*-**P1**(6) is ~60% of that in the absence of PA. In the presence of the same amount of PA, however, the emission of the nanoparticle suspension in the aqueous mixture is almost totally quenched, showing a 69-fold higher sensitivity, in comparison to that of the polymer solution in THF. The nanoaggregates can associate with more PA molecules due to the existence of numerous cavities generated by the loose packing of the globular spheres of *hb*-**P1**(6) containing bulky silole units with twisted molecular conformations. Furthermore, the aggregates offer additional intersphere exciton diffusion pathways. Consequently, the nanoaggregates show a larger PL change or higher sensitivity when exposed to the same amount of explosive analyte.

Different from the conventional linear Stern−Volmer plot, the upward bent curves shown in panels C and D of Figure 17 indicate that the PL quenching becomes more efficient with increasing quencher concentration. As discussed in our recent papers, in comparison to the dynamic quenching model, the static quenching model with an effective quenching sphere is more adequate to describe the quenching behaviors of hyperbranched conjugated polymers,[31,33] because the polymers can function as molecular containers to capture small molecule analytes due to the existence of internal cavities and the potential involvement of Lewis acid−base interactions between the silole moieties and the PA analytes. The preassociation of the PA quenchers with the silole polymers leads to the formation of nonemissive ground-state dark complexes, whereas the unbound polymers exhibit their natural lifetimes. However, in the diffusion-controlled dynamic quenching model, the PL lifetime is shortened with an increase in the quencher concentration.[33] To know which type of the quenching models is at work, the dependence of the lifetime of *hb*-**P1**(6) on the PA concentration is studied. It is found that the lifetime of the polymer is independent of the quencher concentration (Supporting Information, Figure S5). This confirms that the static quenching model is operating in this hyperbranched polymer system, as previously observed in other hyperbranched polymer systems.[31]

In the effective quenching sphere model, I_0/I ratio normally shows an exponential growth dependence on quencher concentration:[33]

$$\frac{I_0}{I} = \mathrm{e}^{V_q[\mathrm{PA}]} \tag{14}$$

where I_0 and I are the fluorescence intensities in the absence and presence of a quencher, respectively, and V_q is the static quenching constant in unit of L mol^{-1}. Mathematical fitting of the I_0/I − [PA] plots shown in panels C and D of Figure 17 gives eqs 15 and 16, respectively:

$$\frac{I_0}{I} = 4.5\mathrm{e}^{333.3[\mathrm{PA}]} - 3.5 \tag{15}$$

$$\frac{I_0}{I} = 2.0\mathrm{e}^{16666.7[\mathrm{PA}]} - 1.0 \tag{16}$$

These two eqs can be generalized as follows:

$$\frac{I_o}{I} = Ae^{V_q[\mathrm{PA}]} + c \tag{17}$$

Compared with eq 14, eqs 15 and 16 show the same trend of single-exponential growth but have two additional constants A and c (eq 17). If we conservatively neglect these two terms, the static quenching constants V_q for the solution and nanoaggregate systems are approximately 333.3 and 16666.7 L mol^{-1}, respectively, which are much higher than those (1−185 L mol^{-1}) reported in the literatures for the linear conjugated iptycene-containing poly(*p*-phenylenebutadiynylene)s and poly(*p*-phenyleneethynylene)s.[34] At low quencher concentrations ([PA] → 0), eqs 15 and 16 can be transformed to eqs 18 and 19 using a mathematical treatment of Taylor expansion:[31]

$$\frac{I_0}{I} - 1 = 1500[\mathrm{PA}] \tag{18}$$

$$\frac{I_0}{I} - 1 = 33333[\mathrm{PA}] \tag{19}$$

The quenching constant for the nanoaggregate system given by eq 19 is 33333 L mol^{-1}, which is more than 22-fold higher than that for its solution counterpart (1500 L mol^{-1}). It is also higher than those for the linear conjugated polysiloles reported in the literature (< 20000 L mol^{-1}).[32] This extremely high quenching efficiency reveals a superamplification effect in the nanoaggregate system.

The superamplification effect is probably associated with the AEE activity of the polymer, its three-dimensional topological structure with numerous internal voids for capturing analyte species and multidimensional migration pathways available to excitons, and the potential involvement of Lewis acid−base interactions between silole units and PA quenchers. All these factors may have worked cooperatively to endow the system with highly sensitive responses to the analytes. It should be pointed out that most conjugated polyelectrolytes unavoidably suffer from the ACQ effect in aqueous media due to the strong $\pi-\pi$ stacking interaction between the hydrophobic conjugated polymer backbones. This effect greatly decreases their sensitivities in real detection systems and often generates false positive signals. The AIE- and AEE-active conjugated polyelectrolytes are thus promising candidate materials for the development of fluorescent chemosensors and bioprobes with superamplified responses effects and extremely low detection limits.

In addition to the solution and suspension in the liquid media, the explosive detection can also be done in the solid state using a polymer-coated strip. For example, a prototype of a solid-state chemosensor is prepared by simply dipping a filter paper into a *hb*-**P1**(6) solution. After solvent evaporation, a highly emissive test paper is obtained. When aliquots of a PA solution are dropped onto the polymer-coated filter paper using a capillary tube, the PA-covered parts become nonemissive. As can be clearly seen from the example shown in the inset of Figure 17C, under UV illumination, the words of "HKUST" written by dropping the PA aliquots onto the filter paper emit no light due to efficient PL quenching by the PA quenchers. These results prompt us to develop ultrasensitive and ultrafast chemosensor devices with portability for on-site detections of explosive vapors and particulates.

Concluding Remarks

In this work, we have succeeded in the first synthesis of a pair of $\sigma-\pi$ conjugated hyperbranched poly(2,5-silole)s *hb*-**P1**(*m*) by the polycyclotrimerization of 2,5-diethynylsiloles **1**(*m*) catalyzed by $TaBr_5$. Polymeric products with high MW (M_w up to $\sim 2.5 \times 10^5$) and most probable DB ($\sim$0.55) are obtained in high yields (up to $\sim$98%). The hyperbranched polysiloles are soluble, durable, stable and processable (film-forming). The absorptions and emissions of *hb*-**P1**(*m*) are red-shifted from those of **1**(*m*) due to the electronic communication between the silole rings and the newly formed benzene rings. Whereas the monomers and the polymers are nonemissive or weakly luminescent when molecularly dissolved in their good solvents, they become highly emissive when aggregated as nanoparticle suspensions in their poor solvents and as thin films in the solid state, showing unique AIE and AEE phenomena. The AIE and AEE effects significantly boost their PL quantum yields by up to 2 orders of magnitude. The RIR process is rationalized to be the main cause for the novel photophysical phenomena.

The emissions of **1**(*m*) and *hb*-**P1**(*m*) can be tuned by varying their concentrations and morphologies. Large blue shifts in the emission colors of the spin-coated films of **1**(*m*)/PMMA (2.5 wt %) blends are observed, implying an unusual shear-induced mechanochromism.[35] Upon heating or photoirradiation, the hyperbranched polymers cross-link into network gels that show excitation wavelength-dependent PL in the red spectral region of 610−735 nm. Photolithography of *hb*-**P1**(*m*) generates fluorescent patterns, in which the exposed and unexposed areas emit lights of different colors. The polymers function as sensitive fluorescent chemosensors for the detection of explosives and a novel superamplification effect is observed in the process of emission quenching of polymer nanoaggregates by PA. These polymers are multifaceted in functionalities and are expected to find an array of technological applications, especially in the area of OLED fabrications and explosive detections.

Experimental Section

General Information. Toluene, hexane, and THF were distilled from sodium benzophenone ketyl immediately prior to use. DCM was distilled over calcium hydride. Triethylamine was distilled under nitrogen and stored over sodium hydroxide in a dark, cold place before use. Tantalum(V) bromide, dichlorobis(triphenylphosphine)palladium(II), $ZnCl_2 \cdot$TMEDA, copper(I) iodide, triphenylphosphine, and other chemicals and solvents were all purchased from Aldrich and used as received without further purification.

$M_{w,r}$ and M_w/M_n values of the polymers were estimated by GPC using a Waters Associates liquid chromatograph equipped with a Waters 515 HPLC pump, a set of Styragel columns (HT3, HT4, and HT6; MW range 10^2-10^7), a column temperature controller, a Waters 486 wavelength-tunable UV−vis detector, a Waters 2414 differential refractometer, and a Waters 2475 fluorescence detector. The polymer solutions were prepared in THF ($\sim$2 mg/mL) and filtered through 0.45-μm PTFE syringe-type filters before being injected into the GPC system. THF was used as eluent at a flow rate of 1.0 mL/min. The column temperature was maintained at 40 °C, and the working wavelength of the UV−vis detector was set at 254 nm. A set of monodisperse polystyrene standards (Waters) covering MW range of 10^3-10^7 were used for MW calibration. $M_{w,a}$ values of *hb*-**P1**(*m*) were measured by commercial laser light scattering (LLS) spectrometer (ALV/DLS/SLS-5022F) equipped with a multi-τ digital time correlator (ALV5000) and a cylindrical 22 mW He−Ne laser (λ_0 = 632 nm, Uniphase) as light source. The $(dn/dC)_{632.8}$ values at 25 °C in THF for *hb*-**P1**(1) and *hb*-**P1**(6) were 0.194 and 0.177 mL/g, respectively, determined by using the Jianke differential refractometer.

Crystals of **1**(1) with quality suitable for X-ray diffraction (XRD) analysis were grown from a 1:1 THF/ethanol mixture. Single crystal XRD intensity data were collected at 173 K on a Bruker-Nonius Smart Apex CCD diffractometer with graphite-monochromated Mo Kα radiation. The data were processed using the SAINT and SADABS routines, and the structure solution and refinement were carried out by the SHELXTL suite of X-ray programs (version 6.10). Particle sizes of the polymers in the THF/water mixtures were measured on a Beckman Coulter Delsa 440SX ζ potential analyzer. IR spectra were recorded on a Perkin-Elmer 16 PC FTIR spectrophotometer. ^{1}H and ^{13}C NMR spectra were measured on a Bruker ARX 400 NMR spectrometer using chloroform-*d* or DCM-d_2 as solvent and tetramethylsilane (TMS) as internal reference. UV absorption spectra were taken on a Milton Ray Spectronic 3000 array spectrophotometer. PL spectra were recorded on a Perkin-Elmer LS 55 spectrofluorometer. Emission efficiencies of thin films of the polymers were measured by a calibrated integrating sphere. High-resolution mass spectra (HRMS) were measured on a GCT Premier CAB 048 mass spectrometer operating in MALDI−TOF model. Thermal stabilities of the monomers and polymers were evaluated on TA Instruments TGA Q5000 and DSC Q1000 under nitrogen at a heating rate of 10 °C/min.

Fluorescence decay curves were recorded on an Edinburgh Instruments FLS920 combined with steady-state and time-resolved fluorescence spectrometers. A femtosecond Ti:sapphire oscillator was used as excitation laser source (200 fs pulse width and 76 MHz repetition rate). The second harmonic (358 nm) of the oscillator output at 716 nm was used for the PL measurement. Time-resolved PL measurements were carried out on a Hamamatsu model C4334 streak camera coupled to a spectrometer, with a time resolution of 20 ps. PL signals were collected at the emission peak at 500 nm and the laser energy level for excitation was 2 mW. Decay in the PL intensity (I) with time (t) was fitted by a double-exponential function (eq 20) and the weighted mean lifetime $\langle\tau\rangle$ was calculated according to eq 21:

$$I = A_1 e^{-t/\tau_1} + A_2 e^{-t/\tau_2} \tag{20}$$

$$\langle\tau\rangle = \frac{A_1\tau_1 + A_2\tau_2}{A_1 + A_2} \tag{21}$$

Thin solid films of *hb*-**P1**(*m*) polymers and **1**(*m*)/PMMA blends were prepared by spin-coating their 1,2-dichloroethane solutions (1.5 wt %) at 800 rpm for 10 s and then 1500 rpm for 60 s on precleaned silicon wafers. The films were dried in a vacuum oven at room temperature to constant weights. The photopattern images of *hb*-**P1**(6) were taken by an OLYMPUS BX41 fluorescence microscope equipped with a SPOT 7.2 color mosaic camera.

Monomer Preparation. 2,5-Diethynylsiloles **1**(*m*) were prepared by a multistep reaction protocol according to the synthetic routes shown in Scheme 1. Typical experimental procedures for the synthesis of the monomers are given below.

Preparation of Dimethylbis(phenylethynyl)silane [**2**(*1*)]. To a THF solution of phenylacetylene (4.0 mL, 36.4 mmol) was added *n*-BuLi (25.0 mL, 40.1 mmol, 1.6 M solution in hexane) at −78 °C. After stirring at −78 °C for 4 h, dichlorodimethylsilane (2.2 mL, 18.2 mmol) was added. The mixture was warmed to room temperature and stirred overnight. The solvent was removed under reduced pressure. The mixture was dissolved in DCM and washed with brine and water. The organic layer was dried over magnesium sulfate. The crude product was purified by a silica-gel column using hexane as eluent. A colorless solid was obtained in 86.1%. ^{1}H NMR (400 MHz, $CDCl_3$), δ (ppm): 7.57 (m, 4H), 7.36 (m, 6H), 0.55 (s, 6H). ^{13}C NMR (100 MHz, $CDCl_3$), δ (ppm): 132.1, 128.9, 128.2, 122.6, 105.9, 90.6, 0.45. HRMS (MALDI−TOF), m/z 260.1013 (M^+, calcd 260.1021).

Preparation of Di(n-hexyl)bis(phenylethynyl)silane [**2**(*6*)]. This compound was prepared using the procedures similar to those for the preparation of **2**(1). A colorless liquid was obtained in 80.3% yield. ^{1}H NMR (400 MHz, $CDCl_3$), δ (TMS, ppm): 7.52 (m, 4H), 7.34 (m, 6H), 1.60 (m, 4H), 1.50−1.20 (m, 12H), 0.8−1.0 (m, 10H). ^{13}C NMR (100 MHz, $CDCl_3$), δ (TMS, ppm): 132.1, 128.7, 128.2, 122.9, 106.6, 89.5, 32.7, 31.5, 23.7, 22.6, 14.8, 14.1. HRMS (MALDI−TOF): *m*/*z* 400.2586 (M^+, calcd 400.2586).

Preparation of 1,1-Dimethyl-2,5-bis[*4-*(*trimethylsilylethynyl*)*-phenyl*]*-3,4-diphenylsilole* [**5**(*1*)]. A mixture of lithium (0.056 g, 8 mmol) and naphthalene (1.04 g, 8 mmol) in 8 mL of THF was stirred at room temperature under nitrogen for 3 h to form a deep dark green solution of LiNaph. The viscous solution was then added dropwise to a solution of **2**(1) (0.52 g, 2 mmol) in 5 mL of THF over 4 min at room temperature. After stirring for 1 h, the mixture was cooled to 0 °C and then diluted with 25 mL THF. A black suspension was formed upon addition of $ZnCl_2$·TMEDA (2 g, 8 mmol). After stirring for an additional hour at room temperature, a solution of [(4-bromophenyl)-ethynyl]trimethylsilane (1.06 g, 4.2 mmol)[13] and $PdCl_2(PPh_3)_2$ (0.08 g, 0.1 mmol) in 25 mL of THF was added. The mixture was refluxed overnight. After cooled to room temperature, 100 mL of 1 M HCl solution was added and the mixture was extracted with DCM. The combined organic layer was washed with brine and water and then dried over magnesium sulfate. After solvent evaporation under reduced pressure, the residue was purified by a silica-gel column using hexane as eluent. The product was obtained as a yellow solid in 71.2% yield. IR (thin film), ν (cm^{-1}): 2156 (C≡C stretching). ^{1}H NMR (400 MHz, CD_2Cl_2), δ (TMS, ppm): 7.17 (m, 4H), 7.00 (m, 6H), 6.84 (m, 4H), 6.78 (m, 4H), 0.43 (s, 6H), 0.19 (s, 18H). ^{13}C NMR (100 MHz, CD_2Cl_2), δ (TMS, ppm): 155.0, 142.1, 140.7, 138.9, 131.7, 130.2, 129.0, 127.8, 126.7, 120.4, 105.5, 94.4, −0.1, −4.1. HRMS (MALDI−TOF): *m*/*z* 606.272 (M^+, calcd 606.259).

Preparation of 1,1-Dihexyl-2,5-bis[*4-*(*trimethylsilylethynyl*)*-phenyl*]*-3,4-diphenylsilole* [**5**(*6*)]. This compound was prepared according to the procedures described above. A yellow solid was obtained in 60.7% yield. IR (thin film), ν (cm^{-1}): 2156 (C≡C stretching). ^{1}H NMR (400 MHz, CD_2Cl_2), δ (ppm): 7.17 (m, 4H), 7.00 (m, 6H), 6.83 (m, 4H), 6.77 (m, 4H), 1.45−1.10 (m, 16H), 0.98 (t, 4H), 0.83 (t, 6H), 0.19 (s, 18H). ^{13}C NMR (100 MHz, CD_2Cl_2), δ (ppm): 156.5, 141.6, 141.4, 139.4, 132.0, 130.5, 129.4, 128.0, 126.9, 120.5, 105.8, 94.6, 33.3, 32.0, 24.0, 23.1, 14.4, 12.4, 0.2. HRMS (MALDI−TOF), *m*/*z* 746.511 (M^+, calcd 746.416).

Synthesis of 1,1-Dimethyl-2,5-bis(*4-ethynylphenyl*)*-3,4-diphenylsilole* [***1***(*1*)]. Into a round-bottomed flask equipped with septum and stirring bar was added **5**(1) (1.21 g, 2 mmol), THF (40 mL), methanol (60 mL), and K_2CO_3 (345 mg, 2.5 mmol). The mixture was stirred at room temperature for 8 h and then neutralized by 3 M HCl solution. The organic solvents were evaporated and the reaction mixture was extracted by DCM three times. The organic layers were combined and after solvent evaporation, the crude product was purified by a silica-gel column using hexane as eluent. A yellow solid was obtained in 96.4% yield. IR (thin film), ν (cm^{-1}): 3291 (≡C−H stretching), 2106 (C≡C stretching). ^{1}H NMR (400 MHz, CD_2Cl_2), δ (TMS, ppm): 7.21 (m, 4H), 7.00 (m, 6H), 6.86 (m, 4H), 6.79 (m, 4H), 3.06 (s, 2H), 0.44 (s, 6H). ^{13}C NMR (100 MHz, CD_2Cl_2), δ (TMS, ppm): 155.3, 142.3, 141.3, 139.1, 132.2, 130.4, 129.3, 128.0, 127.0, 119.5, 84.2, 77.5, −3.9. HRMS (MALDI−TOF), *m*/*z* 462.1821 (M^+, calcd 462.1804).

Synthesis of 1,1-Dihexyl-2,5-bis(*4-ethynylphenyl*)*-3,4-diphenylsilole* [***1***(*6*)]. This monomer was synthesized using the procedures similar to those for the preparation of **1**(1). A yellow viscous liquid was obtained in 95.5% yield. IR (thin film), ν (cm^{-1}): 3294 (≡C−H stretching), 2107 (C≡C stretching). ^{1}H NMR (400 MHz, CD_2Cl_2), δ (TMS, ppm): 7.21 (m, 4H), 7.00 (m, 6H), 6.86 (m, 4H), 6.79 (m, 4H), 3.06 (s, 2H), 1.45−1.10 (m, 16H), 0.99 (t, 4H), 0.83 (t, 6H). ^{13}C NMR (100 MHz, CD_2Cl_2), δ (TMS, ppm): 156.6, 141.9, 141.3, 139.3, 132.2, 130.4, 129.4, 128.0, 127.0, 119.4, 84.3, 77.5, 33.3, 32.0, 24.1, 23.1, 14.4, 12.4. HRMS (MALDI−TOF), *m*/*z* 602.342 (M^+, calcd 602.337).

Polymer Synthesis. All the polymerization reactions were carried out under nitrogen using standard Schlenk technique in a vacuum line system or an inert atmosphere glovebox. A typical experimental procedure for the polycyclotrimerization of **1**(1) is given below.

To a thoroughly baked and carefully evacuated 15 mL Schlenk tube with a three-way stopcock on the side arm was placed 8.7 mg (0.015 mmol) of $TaBr_5$ under nitrogen in a glovebox. Freshly distilled toluene (2.0 mL) was then injected into the tube using a hypodermic syringe. After aging for 5 min at 80 °C, a solution of 69.4 mg (0.15 mmol) of **1**(1) in 1.0 mL of toluene was injected. The resultant mixture was stirred at room temperature under nitrogen for 0.5 h and the polymerization was then quenched by the addition of a small amount of methanol. The solution was added dropwise to 300 mL of methanol through a cotton filter under stirring. The precipitate was allowed to stand overnight and then collected by filtration. The polymer was washed with methanol and dried under vacuum at room temperature to a constant weight.

Characterization Data for hb-P1(*1*). Yellow powder; yield: 75.6%. $M_{w,r}$ 17600; M_w/M_n 3.2 (Table 1, no. 2). IR (thin film), ν (cm^{-1}): 3291 (≡C−H stretching), 2106 (C≡C stretching). ^{1}H NMR (300 MHz, CD_2Cl_2), δ (TMS, ppm): 6.70−8.40 (Ar−H), 3.07 (≡C−H), 0.45 [$Si(CH_3)_2$]. ^{13}C NMR (75 MHz, CD_2Cl_2), δ (TMS, ppm): 119.0−158.0 (aromatic carbons), 84.2 (*C*≡CH), 77.5 (C≡*C*H), −3.9 [$Si(CH_3)_2$].

Characterization Data for hb-P1(*6*). Yellow powder; yield: 97.9%. $M_{w,r}$ 27600; M_w/M_n 4.1 (Table 1, no. 3). IR (thin film), ν (cm^{-1}): 3294 (≡C−H stretching), 2107 (C≡C stretching). ^{1}H NMR (400 MHz, CD_2Cl_2), δ (TMS, ppm): 6.70−8.00 (Ar−H), 3.07 (≡C−H), 0.5−1.8 [$Si(CH_2CH_2CH_2CH_2CH_2CH_3)_2$]. ^{13}C NMR (100 MHz, CD_2Cl_2), δ (TMS, ppm): 119.0−158.0 (aromatic carbons), 84.3 (*C*≡CH), 77.5 (C≡*C*H), 33.3, 32.0, 24.1, 23.1, 14.5, 12.5 [$Si(CH_2CH_2CH_2CH_2CH_2CH_3)_2$].

Acknowledgment. The work described in this paper was partially supported by the Research Grants Council of Hong Kong (603509 and 603008), the University Grants Committee of Hong Kong (AoE/P-03/08), the Innovation and Technology Fund of Hong Kong (ITP/008/09NP and ITS/168/09), the National Natural Science Foundation of China (20634020 and 20974028), and the Ministry of Science and Technology of China (2009CB623605). BZT thanks the support from Cao Gaungbiao Foundation of Zhejiang University.

Supporting Information Available: Table of crystal structural parameters of **1**(1) and figures showing GPC traces of *hb*-**P1**(*m*), UV absorption spectra of **1**(*m*) and *hb*-**P1**(*m*) in THF/water mixtures with 90 vol % water, IR spectra of **1**(1) before and after thermal treatment and UV irradiation, excitation wavelength-dependent emission spectra of UV irradiated thin film of *hb*-**P1**(6), and fluorescence decay curves of *hb*-**P1**(6) in the presence of different amounts of picric acid in THF, and a .cif file containg crystallographic resuts for **1**(1). This material is available free of charge via the Internet at http://pubs.acs.org.

References and Notes

(1) Birks, J. B. *Photophysics of Aromatic Molecules*: Wiley: London, 1970.
(2) Luo, J. D.; Xie, Z. L.; Lam, J. W. Y.; Cheng, L.; Chen, H. Y.; Qiu, C. F.; Kwok, H. S.; Zhan, X. W.; Liu, Y. Q.; Zhu, D. B.; Tang, B. Z. *Chem. Commun.* **2001**, 1740.
(3) For reviews, see: (a) Hong, Y.; Lam, J. W. Y.; Tang, B. Z. *Chem. Commun.* **2009**, 4332. (b) Liu, J.; J. W. Y.; Tang, B. Z. *J. Inorg. Organomet. Polym. Mater.* **2009**, *19*, 249. (c) Wang, M.; Zhang, G.; Zhang, D.; Zhu, D.; Tang, B. Z. *J. Mater. Chem.* **2010**, *20*, 1858.

(d) Yan, J.; Sun, J.; Qin, A.; Tang, B. Z. *Chin. Sci. Bull.* **2010**, *55*, DOI: 10.1360/972009-2307.
(4) (a) Chen, J.; Law, C. W.; Lam, J. W. Y.; Dong, Y.; Lo, S. M. F.; Williams, I. D.; Zhu, D.; Tang, B. Z. *Chem. Mater.* **2003**, *15*, 1535. (b) Zhao, Z.; Wang, Z.; Lu, P.; Chan, C. Y. K.; Liu, D.; Lam, J. W. Y.; Sung, H. H. Y.; Williams, I. D.; Ma, Y.; Tang, B. Z. *Angew. Chem.−Int. Ed.* **2009**, *48*, 7608. (c) Yuan, W. Z.; Lu, P.; Chen, S.; Lam, J. W. Y.; Wang, Z.; Liu, Y.; Kowk, H. S.; Ma, Y.; Tang, B. Z. *Adv. Mater.* **2010**, *22*, DOI: 10.1002/adma.200904056.
(5) (a) Peng, Q.; Yi, Y.; Shuai, Z.; Shao, J. *J. Am. Chem. Soc.* **2007**, *129*, 9333. (b) Yin, S.; Peng, Q.; Shuai, Z.; Fang, W.; Wang, Y. H.; Luo, Y. *Phys. Rev. B* **2006**, *73*, 205409.
(6) (a) An, B.-K.; Kwon, S.-K.; Jung, S.-D.; Park, S. Y. *J. Am. Chem. Soc.* **2002**, *124*, 14410. (b) Yeh, H. C.; Yeh, S. J.; Chen, C. T. *Chem. Commun.* **2003**, 2632. (c) Chen, J.; Xu, B.; Ouyang, X.; Tang, B. Z.; Cao, Y. *J. Phys. Chem. A* **2004**, *108*, 7522. (d) Tracy, H. J.; Mullin, J. L.; Klooster, W. T.; Martin, J. A.; Haug, J.; Wallace, S.; Rudloe, I.; Watts, K. *Inorg. Chem.* **2005**, *44*, 2003. (e) Toal, S. J.; Jones, K. A.; Magde, D.; Trogler, W. C. *J. Am. Chem. Soc.* **2005**, *127*, 11661. (f) Wang, Z.; Shao, H.; Ye, J.; Tang, L.; Lu, P. *J. Phys. Chem. B* **2005**, *109*, 19627. (g) Yu, G.; Yin, S.; Liu, Y. Q.; Chen, J.; Xu, X.; Sun, X.; Ma, D.; Zhan, X.; Peng, Q.; Shuai, Z. G.; Tang, B. Z.; Zhu, D. B.; Fang, W.; Luo, Y. *J. Am. Chem. Soc.* **2005**, *127*, 6335. (h) Lee, S. H.; Jang, B. B.; Kafafi, Z. H. *J. Am. Chem. Soc.* **2005**, *127*, 9071. (i) Sun, Y. Y.; Liao, J. H.; Fang, J. M.; Chou, P. T.; Shen, C. H.; Hsu, C. W.; Chen, L. C. *Org. Lett.* **2006**, *8*, 3713. (j) Han, M. R.; Hirayama, Y.; Hara, M. *Chem. Mater.* **2006**, *18*, 2784. (k) Bao, C. Y.; Lu, R.; Jin, M.; Xue, P. C.; Tan, C. H.; Xu, T. H.; Liu, G. F.; Zhao, Y. Y. *Chem.—Eur. J.* **2006**, *12*, 3287. (l) Bhongale, C. J.; Hsu, C.-S. *Angew. Chem., Int. Ed.* **2006**, *45*, 1404. (m) Kim, S.; Zheng, Q.; He, G. S.; Bharali, D. J.; Pudavar, H. E.; Baev, A.; Prasad, P. N. *Adv. Funct. Mater.* **2006**, *16*, 2317. (n) Li, Y.; Li, F.; Zhang, H.; Xie, Z.; Xie, W.; Xu, H.; Li, B.; Shen, F.; Ye, L.; Hanif, M.; Ma, D.; Ma, Y. *Chem. Commun.* **2007**, 231. (o) Kim, J.-M. *Macromol. Rapid Commun.* **2007**, *28*, 1191. (p) Qian, Y.; Li, S.; Zhang, G.; Wang, Q.; Wang, S.; Xu, H.; Li, C.; Li, Y.; Yang, G. *J. Phys. Chem. B.* **2007**, *111*, 5861. (q) Li, C.; Liu, X.; Yuan, M.; Li, J.; Guo, Y.; Xu, J.; Zhu, M.; Lv, J.; Liu, H.; Li, Y. *Langmuir* **2007**, *23*, 6754. (r) Ning, Z.; Chen, Z.; Zhang, Q.; Yan, Y.; Qian, S.; Cao, Y.; Tian, H. *Adv. Funct. Mater.* **2007**, *17*, 3799. (s) Zhao, M. C.; Wang, M.; Liu, H.; Liu, D. S.; Zhang, G. X.; Zhang, D. Q.; Zhu, D. B. *Langmuir* **2009**, *25*, 676. (t) Yuan, C. X.; Tao, X. T.; Wang, L.; Yang, J. X.; Jiang, M. H. *J. Phys. Chem. C* **2009**, *113*, 6809. (u) Wu, Y. T.; Kuo, M. Y.; Chang, Y. T.; Shin, C. C.; Wu, T. C.; Tai, C. C.; Cheng, T. H.; Liu, W. S. *Angew. Chem., Int. Ed.* **2008**, *47*, 9891. (v) Wang, M.; Gu, X. G.; Zhang, G. X.; Zhang, D. Q.; Zhu, D. B. *Anal. Chem.* **2009**, *81*, 4444. (w) Dong, J.; Solntsev, K. M.; Tolbert, L. M. *J. Am. Chem. Soc.* **2009**, *131*, 662. (x) Pu, K. Y.; Liu, B. *Adv. Funct. Mater.* **2009**, *19*, 277.
(7) Chen, H. Y.; Lam, W. Y.; Luo, J. D.; Ho, Y. L.; Tang, B. Z.; Zhu, D. B.; Wong, M.; Kwok, H. S. *Appl. Phys. Lett.* **2002**, *81*, 574.
(8) (a) Tamao, K.; Yamaguchi, S.; Shiozaki, M.; Nakagawa, Y.; Ito, Y. *J. Am. Chem. Soc.* **1992**, *114*, 5867. (b) Lee, Y.; Sadki, S.; Tsuie, B.; Reynolds, J. R. *Chem. Mater.* **2001**, *13*, 2234. (c) Yamaguchi, S.; Goto, K.; Tamao, K. *Angew. Chem., Int. Ed.* **2000**, *39*, 1695. (d) Corriu, R. J. -P.; Douglas, W. E.; Yang, Z. -X. *J. Organomet. Chem.* **1993**, *465*, 35. (e) Toyoda, E.; Kunai, A.; Ishikawa, M. *Organometallics* **1995**, *14*, 1089. (f) Sanji, T.; Sakai, T.; Kabuto, C.; Sakurai, H. *J. Am. Chem. Soc.* **1998**, *120*, 4552. (g) Yamaguchi, S.; Jin, R, -Z.; Itami, Y.; Goto, T.; Tamao, K. *J. Am. Chem. Soc.* **1999**, *121*, 10420.
(9) (a) Liu, J. Z.; Lam, J. W. Y.; Tang, B. Z. *Chem. Rev.* **2009**, *109*, 5799. (b) Tang, B. Z. *Macromol. Chem. Phys.* **2008**, *209*, 1303.
(10) Lam, J. W. Y.; Tang, B. Z. *Acc. Chem. Res.* **2005**, *38*, 745.
(11) (a) Qin, A.; Lam, J. W. Y.; Tang, B. Z. *Chem. Soc. Rev.* **2010**, *39*, DOI: 10.1039/b909064a.(b) Qin, A.; Tang, L.; Lam, J. W. Y.; Jim, C. K. W.; Yu, Y.; Zhao, H.; Sun, J. Z.; Tang, B. Z. *Adv. Funct. Mater.* **2009**, *19*, 1891.
(12) Häussler, M.; Tang, B. Z. *Adv. Polym. Sci.* **2007**, *209*, 1.
(13) Liu, J. Z.; Zheng, R. H.; Tang, Y. H.; Haussler, M.; Lam, J. W. Y.; Qin, A.; Ye, M. X.; Hong, Y. N.; Gao, P.; Tang, B. Z. *Macromolecules* **2007**, *40*, 7473.
(14) (a) Jim, C. K. W.; Qin, A.; Lam, J. W. Y.; Haussler, M.; Liu, J.; Yuen, M. M. F.; Kim, J. K.; Ng, K. M.; Tang, B. Z. *Macromolecules* **2009**, *42*, 4099. (b) Häussler, M.; Qin, A.; Tang, B. Z. *Polymer* **2007**, *48*, 6181. (c) Chen, J. W.; Peng, H.; Law, C. C. W.; Dong, Y. P.; Lam, J. W. Y.; Williams, I. D.; Tang, B. Z. *Macromolecules* **2003**, *36*, 4319.
(15) Braye, E. H.; Hubel, W. *Chem. Ind.* **1959**, 1250.
(16) For reviews, see: (a) Moustafa, M.; Pagenkopf, B. L. *C. R. Chim.* **2009**, *12*, 359. (b) Hill, N. J.; West, R. *J. Organomet. Chem.* **2004**, *689*, 4165. (c) Lee, V. Y.; Sekiguchi, A.; Ichinohe, M.; Fukaya, N. *J. Organomet. Chem.* **2000**, *611*, 228. (d) Haaf, M.; Schmedake, T. A.; West, R. *Acc. Chem. Res.* **2000**, *33*, 704. (e) Hermanns, J.; Schmidt., B. *J. Chem. Soc., Perkin Trans. 1* **1999**, 81. (f) Yamaguchi, S.; Tamao, K. *J. Chem. Soc., Dalton Trans.* **1998**, 3693. (h) Chen, J. W.; Cao, Y. *Macromol. Rapid Commun.* **2007**, *28*, 1714. (i) Tamao, K.; Yamaguchi, S. *J. Organomet. Chem.* **2000**, *611*, 5. (j) Sanchez, J. C.; Trogler, W. C. *Macromol. Chem. Phys.* **2008**, *209*, 1528.
(17) (a) Booker, C.; Wang, X.; Haroun, S.; Zhou, J. G.; Jennings, M.; Pagenkopf, B. L.; Ding, Z. F. *Angew. Chem., Int. Ed.* **2008**, *47*, 7731. (b) Toulokhonova, I. S.; Friedrichsen, D. R.; Hill, N. J.; Muller, T.; West, R. **2006**, *45*, 2578.(c) Sartin, M. M.; Boydston, A. J.; Pagenkopf, B. L.; Bard, A. J. *J. Am. Chem. Soc.* **2006**, *128*, 10163. (d) Lee, J.; Yuan, Y.; Kang, Y.; Jia, W.; Lu, Z.; Wang, S. *Adv. Funct. Mater.* **2006**, *16*, 681. (e) Boydston, A. J.; Yin, Y. S.; Pagenkopf, B. L. *J. Am. Chem. Soc.* **2004**, *126*, 10350. (f) Lee, J.; Liu, Q.; Bai, D.; Kang, Y.; Tao, Y.; Wang, S. *Organometallics* **2004**, *23*, 6205. (g) Boydston, A. J.; Yin, Y.; Pagenkopf, B. L. *J. Am. Chem. Soc.* **2004**, *126*, 3724. (h) Kim, W.; Palilis, L. C.; Uchida, M.; Kafafi, Z. H. *Chem. Mater.* **2004**, *16*, 4681. (i) Yamaguchi, S.; Endo, T.; Uchida, M.; Izumizawa, T.; Furukawa, K.; Tamao, K. *Chem.—Eur. J.* **2000**, *6*, 1683. (j) Wang, C.; Luo, Q.; Sun, H.; Guo, X.; Xi, Z. *J. Am. Chem. Soc.* **2007**, *129*, 3094. (k) IIies, L.; Tsuji, H.; Nakamura, E. *Org. Lett.* **2009**, *11*, 3966.
(18) (a) Tamao, K.; Yamaguchi, S.; Shiro, M. *J. Am. Chem. Soc.* **1994**, *116*, 11715. (b) Tamao, K.; Uchida, M.; Izumizawa, T.; Furukawa, K.; Yamaguchi, S. *J. Am. Chem. Soc.* **1996**, *118*, 11974.
(19) (a) Hawker, C. J.; Malmstrom, E. E.; Curtis, W. F.; Kampf, J. P. *J. Am. Chem. Soc.* **1997**, *119*, 9903. (b) Harth, E. M.; Hecht, S.; Helms, B.; Malmstrom, E. E.; Frechet, J. M. J.; Hawker, C. J. *J. Am. Chem. Soc.* **2002**, *124*, 3926.
(20) (a) Irzhak, T. F.; Irzhak, V. I.; Malkov, G. V.; Estrin, Ya. I.; Badamshina, E. R. *Polym. Sci., Ser. B* **2009**, *51*, 183. (b) Irzhak, T. F.; Irzhak, V. I.; Malkov, G. V.; Estrin, Ya. I.; Badamshina, E. R. *Polym. Sci., Ser. A* **2008**, *50*, 74.
(21) (a) Hawker, C. J.; Lee, R.; Frechet, J. M. J. *J. Am. Chem. Soc.* **1991**, *113*, 4583. (b) Frey, H.; Hoelter, D. *Acta Polym.* **1999**, *50*, 67.
(22) (a) Yan, D.; Muller, A. H. E.; Matyjaszewski, K. *Macromolecules* **1997**, *30*, 7024. (b) Holter, D.; Burgath, A.; Frey, H. *Acta Polym.* **1997**, *48*, 30. (c) Holter, D.; Frey, H. *Acta Polym.* **1997**, *48*, 298. (d) Gao, C.; Yan, D. *Prog. Polym. Sci.* **2004**, *29*, 183. (e) Tomalia, D. A.; Fréchet, J. M. *J. Polym. Sci., Part A: Polym. Chem.* **2002**, *40*, 2719. (f) Jikei, M.; Kakimoto, M. *Prog. Polym. Sci.* **2001**, *26*, 1233. (g) Kim, Y. H. *J. Polym. Sci., Part A: Polym. Chem.* **1998**, *36*, 1685. (h) Voit, B. *J. Polym. Sci., Part A: Polym. Chem.* **2000**, *38*, 2505. (i) Pattern, T. E.; Matyjaszewski, K. *Adv. Mater.* **1998**, *10*, 901.
(23) Hergenrother, P. M. In *Concise Encyclopedia of Polymer Science and Engineering*; Kroschwitz, J. I., Ed.; Wiley: New York, 1990.
(24) Zhao, Z.; Chen, S.; Lam, J. W. Y.; Jim, C. K. W.; Chan, C. Y. K.; Wang, Z.; Lu, P.; Deng, C.; Kwok, H. S.; Ma, .Y.; Tang, B. Z. *J. Phys. Chem. C* **2010**, *114*, DOI: 10.1021/jp910728x.
(25) Frisch, M. J. et al. *Gaussian 03, rev B.01*; Gaussian, Inc.: Pittsburgh, PA, 2003.
(26) Zhao, Z.; Chen, S.; Shen, X.; Mahtab, F.; Yu, Y.; Lu, P.; Lam, J. W. Y.; Kwok, H. S.; Tang, B. Z. *Chem. Commun.* **2010**, *46*, 686.
(27) Ren, Y.; Lam, J. W. Y.; Dong, Y. Q.; Tang, B. Z.; Wong, K. S. *J. Phys. Chem. B* **2005**, *109*, 1135.
(28) Dong, Y. Q.; Lam, J. W. Y.; Li, Z.; Qin, A. J.; Tong, H.; Dong, Y. P.; Feng, X. D.; Tang, B. Z. *J. Inorg. Organomet. Polym. Mater.* **2005**, *15*, 287.
(29) (a) Kim, J. M. *Macromol. Rapid Commun.* **2007**, *28*, 1191. (b) Lam, J. W. Y.; Tang, B. Z. *J. Polym. Sci., Part A: Polym. Chem.* **2003**, *41*, 2607. (c) Campbell, L.; Sharp, D. N.; Harrison, M. T.; Denning, R. G.; Turberfield, A. J. *Nature* **2000**, *404*, 53.
(30) (a) Tyler McQuade, D.; Pullen, A. E.; Swager, T. M. *Chem. Rev.* **2000**, *100*, 2537. (b) Thomas Iii, S. W.; Joly, G. D.; Swager, T. M. *Chem. Rev.* **2007**, *107*, 1339. (c) Yinon, J. *Anal. Chem.* **2003**, *75*, 99A. (d) Moore, D. S. *Rev. Sci. Instrum.* **2004**, *75*, 2499. (e) Bunz, U. H. F. *Chem. Rev.* **2000**, *100*, 1605. (f) Zahn, S.; Swager, T. M. *Angew. Chem., Int. Ed.* **2002**, *41*, 4226. (g) Liu, Y.; Mills, R. C.; Boncella, J. M.; Schanze, K. S. *Langmuir* **2001**, *17*, 7452. (h) Huang, H. M.; Wang, K. M.; Xiao, D.; Yang, R. H.; Yang, X. H. *Anal. Chim. Acta* **2001**, *439*, 55. (i) Chang, C. P.; Chao, C. Y.; Huang, J. H.; Li, A. K.; Hsu, C. S.; Lin, M. S.; Hsieh, B. R.; Su, A. C. *Synth. Met.* **2004**, *144*, 297. (j) Kim, T. H.; Kim, H. J.; Kwak, C. G.; Park, W. H.; Lee, T. S. *J. Polym. Sci., Part A: Polym. Chem.* **2006**, *44*, 2059. (k) Naddo, T.; Che, Y.; Zhang, W.; Balakrishnan, K.; Yang, X.; Yen, M.; Zhao, J.; Moore, J. S.; Zhang, L. *J. Am. Chem. Soc.* **2007**, *129*, 6978. (l) Germain, M. E.; Knapp, M. J. *J. Am. Chem. Soc.* **2008**, *130*, 5422. (m) Hughes, A. D.;

Glenn, I. C.; Patrick, A. D.; Ellington, A.; Anslyn, E. V. *Chem.—Eur. J.* **2008**, *14*, 1822. (n) Jiang, Y.; Zhao, H.; Zhu, N.; Lin, Y.; Yu, P.; Mao, L. *Angew. Chem., Int. Ed.* **2008**, *47*, 8601. (o) Shiraishi, K.; Sanji, T.; Tanaka, M. *ACS Appl. Mater. Interface* **2009**, *1*, 1379. (p) Long, Y.; Chen, H.; Yang, Y.; Wang, H.; Yang, Y.; Li, N.; Li, K.; Pei, J.; Liu, F. *Macromolecules* **2009**, *42*, 6501.

(31) (a) Liu, J.; Zhong, Y.; Lu, P.; Hong, Y.; Lam, J. W. Y.; Faisal, M.; Yu, Y.; Wong, K. S.; Tang, B. Z. *Polym. Chem.* **2010**, 1, DOI: 10.1039/c0py00046a. (b) Lu, P.; Lam, J. W. Y.; Liu, J.; Jim, C. K. W.; Yuan, W.; Xie, N.; Zhong, Y.; Hu, Q.; Wong, K. S.; Cheuk, K. K. L.; Tang, B. Z. *Macromol. Rapid Commun.* **2010**, *31*, DOI: 10.1002/marc.200900794.

(32) (a) Sanchez, J. C.; Urbas, S. A.; Toal, S. J.; DiPasquale, A. G.; Rheingold, A. L.; Trogler, W. C. *Macromolecules* **2008**, *41*, 1237. (b) Sanchez, J. C.; DiPasquale, A. G.; Rheingold, A. L.; Trogler, W. C. *Chem. Mater.* **2007**, *19*, 6459.

(33) Valeur, B. *Molecular Fluorescence: Principle and Applications*; Wiley−VCH: Weinheim, Germany, 2002.

(34) Zhao, D.; Swager, T. M. *Macromolecules* **2005**, *38*, 9377.

(35) Lott, J.; Weder, C. *Macromol. Chem. Phys.* **2010**, *211*, 28.